Contrib Mineral Petrol (2007) 154:55–74
DOI 10.1007/s00410-006-0179-z

ORIGINAL PAPER

Rare earth element fractionation in magmatic Ca-rich garnets

Birgit Scheibner · Gerhard Wörner · Lucia Civetta · Heinz- Günter Stosch · Klaus Simon · Andreas Kronz

Received: 30 June 2006 / Accepted: 19 December 2006 / Published online: 23 February 2007

Abstract Igneous garnets have the potential to strongly fractionate rare earth elements (REE). Yet informations on partition coefficients are very scant, and criteria for distinguishing between hydrothermal and magmatic garnets are ambiguous. To fill this gap, we present trace element and isotopic data for two types of Ca-rich garnets from phonolites (Mt. Somma-Vesuvius). Both Ca-garnet populations are different in their style and dynamics of fractionation: one population is progressively strongly depleted in HREE from core to rim, reflecting REE fractionation in the host phonolite via earlier-crystallized garnets. Such examples for extreme changes in HREE in garnets are only known for hydrothermal grandites by REE-bearing fluids. The second garnet population is homogeneous and formed in a closed system. Near-flat patterns between Sm and Lu confirm experimental data indicating lower D(Sm)/D(Lu) for Ca-rich garnets than for e.g. pyrope-rich garnets. It follows: $D^{\mathrm{Grt/PhMelt}}$ for La = 0.5, Sm = 48 and Yb = 110.

Keywords Grandite · Ca-rich garnets · Andradite · Rare earth elements · Mt. Somma-Vesuvius · Fractionation · Partition coefficient · Skarn · Hydrothermal · Magma chamber · Phonolite

Communicated by T. L. Grove.

B. Scheibner (✉) · G. Wörner · K. Simon · A. Kronz
Geowissenschaftliches Zentrum Göttingen (GZG)—Geochemie, Universität Göttingen, Goldschmidtstr. 1, 37077 Göttingen, Germany
e-mail: B.Scheibner@gmx.de; B.Scheibner@fz-juelich.de

B. Scheibner
Forschungszentrum Jülich, Neue Materialien und Chemie, Wilhelm-Johnen-Straße 12, 52428 Jülich, Germany

L. Civetta
Instituto Nazionale di Geofisica e Vulcanologia, Osservatorio Vesuviano and Department Scienze Fisiche, Universitá di Napoli Federico II, Via Diocleziano 328, 80124 Naples, Italy

H.-G. Stosch
Institut für Mineralogie und Geochemie, Universität Karlsruhe (TH), Fritz-Haber-Weg 2, D-76131 Karlsruhe, Germany

Introduction

The effect of garnet on the trace element compositions of mantle-derived melts, in particular their strong preference for heavy rare earth elements (HREE) has long been known and was demonstrated in various experimental studies (e.g. Hauri et al. 1994; Johnson 1998; Salters and Longhi 1999; Pertermann et al. 2004). Furthermore, recent studies suggest a different fractionation behaviour for HREE in garnets of different major element compositions (Westrenen et al. 1999, 2001). In contrast to mantle garnets or metamorphic garnets, partitioning data for magmatic garnets from highly differentiated magma compositions are still scarce (Irving and Frey 1978; Sisson and Bacon 1992), and data from phonolitic melts were previously not available.

For the determination of partitioning data in a natural system, however, it is essential to distinguish, whether the garnets of a phonolite sample are juvenile igneous garnet phenocrysts or residual xenocrysts formed, for example, during hydrothermal processes.

This distinction is necessary because in a phonolitic volcanic system in contact with carbonate host rocks, both hydrothermal garnets in the calcareous wall rock during skarn-forming processes and magmatic garnets crystallizing from the phonolitic magma may be formed. The incorporation of the hydrothermal xenocrysts into the phonolite melt may occur during magma emplacement into the country rock.

Both metasomatic and true magmatic Ca-rich garnets are in fact similar in their chemical and mineralogical composition. A comparison of igneous and metasomatic andradite-grossularite garnets with respect to chemical zonation, colour and trace element content (Table 1) shows that the discrimination of these two types of garnets is not straightforward, and a combination of various geochemical and textural parameters are required to distinguish their genesis.

Phonolites from the Mt. Somma-Vesuvius region (Southern Italy, Fig. 1) are ideally suited for such a study. Garnets from Mt. Somma-Vesuvius occur in a silica-undersaturated, phonolitic magma in association with a skarn-forming environment (Fig. 2). Metasomatic carbonates and skarn xenoliths, found in Mt. Somma-Vesuvius volcanic rocks (Gilg et al. 2001), suggest the presence of a large skarn aureole surrounding the Mt. Somma-Vesuvius magma chamber. There is consensus (Fulignati et al. 2005) that such an aureole of Ca–Fe–Mg-rich silicate rocks was formed below Mt. Somma-Vesuvius at 3–6 km depth (Zollo 1996; Cioni 2000) by metasomatism of Cretaceous limestones and Triassic dolomites. This metasomatic process replaced the original carbonate by a calc-silicate mineral assemblage including garnet, pyroxene, spinel (Fulignati et al. 2004), as well as REE-, U-, Th-, Zr- and Ti-rich accessory minerals (Gilg et al. 2001). However, several processes are considered with respect to the origin of Mt. Somma-Vesuvius garnets: (1) magmatic crystallisation, (2) post-magmatic pneumatolitic processes or (3) assimilation of skarn-related xenocrystic garnets.

The aim of this study is first to provide evidence for distinguishing between these potential types of garnets in two Vesuvius phonolites (Mercato and Avellino eruption) by comparing, for example, trace element as well as Sr and O-isotope compositions of host melt and garnets. Based on these data, we propose an igneous origin of the grandites as phenocrysts for the two phonolites This conclusion is important for determining the first empirical crystal/liquid partition coefficients for rare earth elements (REE) between Ca-rich garnets and phonolitic melt in a natural system and for modelling the trace element evolution of garnets and melts during growth and progressive HREE-depletion of the co-existing melt. Up to the present, such a detailed growth history for Ca-rich garnets with regard to their REE budget has only been reported from hydrothermal Ca-rich garnets (e.g. Smith et al. 2004). Our study also evaluates the HREE partitioning in grossularite-rich

Table 1 Origin and occurrence of titanian andradites in different environments

Type of garnet	Origin	Occurrence	Zoning	TiO_2 (%)	Reference
Metamorphic, metasomatic, and/or hydrothermal origin					
$And_{88}Gro_{12}$	Thermo-Metamorphic?	Somma-Vesuvius (South Italy)	Unzoned	1.8	Naimo et al. (2003)
$And_{82}Gro_{18}$	Hydrothermal associated with alkaline intrusions	Galore Creek (Canadian Cordillera)	Zoned	2.0	Russell et al. (1999)
$And_{96}Gro_{4}$	Serpentinites	San Benito (CA, USA)	Zoned	8.9	Armbruster et al. (1998)
$And_{93}Gro_{7}$ to And_{100}	Metasomatic/ hydrothermal (skarn)	Beinn an Dubhaich Aureole, Skye (Scotland, UK)	Zoned	<0.01	Smith et al. (2004)
$And_{98}Gro_{2}$	Metasomatic/ hydrothermal (skarn)	Beinn an Dubhaich Aureole, Skye (Scotland, UK)	Unzoned	0.02	Smith et al. (2004)
$And_{28}Gro_{70}$	Metasomatic/ hydrothermal (skarn)	79 A.D. Pompei, Somma-Vesuvius (South Italy)	Zoned	0.84–0.98	Fulignati et al. (2004)
Igneous origin					
$And_{90}Gro_{10}$	Trachyte dyke	Rugged Mountain (Canadian Cordillera)	Zoned	5.4	Russell et al. (1999)
$And_{88}Gro_{12}$	Phonolite dyke	Kaiserstuhl (Germany)	Unzoned	12.4	Armbruster et al. (1998)
$And_{66}Gro_{34}$	Phonolite/trachyte	Mt. Vulture (South Italy)	Unzoned?	3.0	Scordari et al. (1999)
$And_{68}Gro_{26}$	Phonolite	79 A.D. Somma-Vesuvius (South Italy)	–	2.9	Cioni et al. (1995)
Post-magmatic origin					
$And_{3}Gro_{97}$	Post-magmatic	Phlegraean Fields (South Italy)	Unzoned	0.2–0.7	Naimo et al. (2003)
$And_{99}Gro_{1}$	Post-magmatic	Phlegraean Fields (South Italy)	Unzoned	0.07–0.1	Naimo et al. (2003)

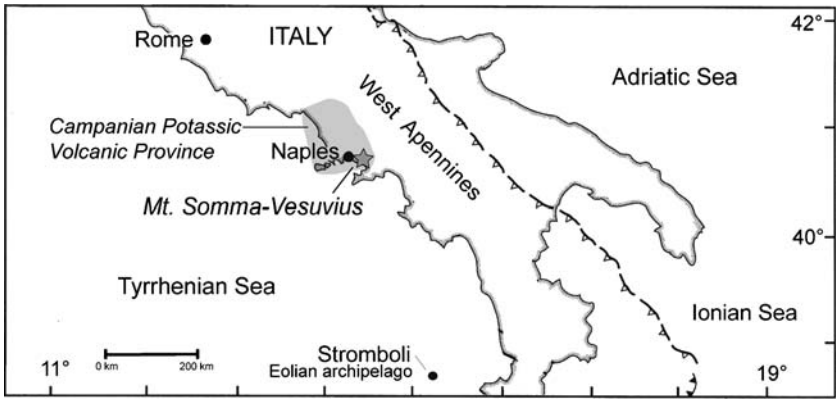

Fig. 1 Location map for the Mt. Somma-Vesuvius volcanic complex and the Campanian Potassic Volcanic Province in the western Apennines. Volcanic activity of Southern Italy is triggered by the northwards subducting Ionian slab and extension movements in the Tyrrhenian Sea. *Star* Mt. Somma-Vesuvius, *grey field* Campanian Potassic Volcanic Province, *dashed line* subducting Ionian slap (map modified after Elter et al. 2003)

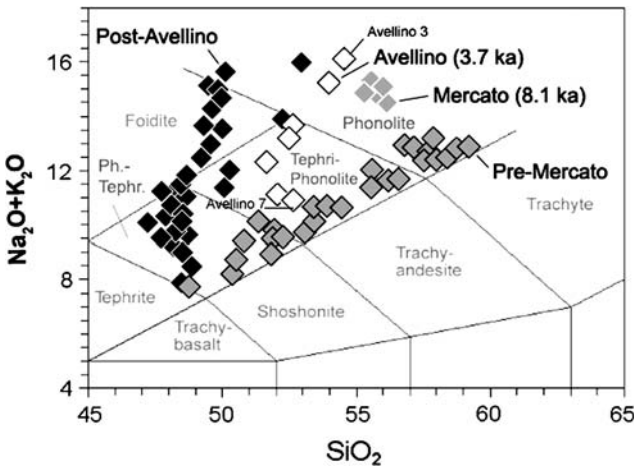

Fig. 2 Geochemical classification of the activity of Mt. Somma-Vesuvius on the basis of Ayuso et al. (1998). Avellino and Mercato pumices belong to Group II of that classification. *White diamonds* Avellino, *grey diamonds and black rim* Pre-Mercato, *grey diamonds and white rim* Mercato, *black diamonds and white rim* Post-Avellino

garnets with respect to the fractionation behaviour of pyrope-rich garnets.

Samples and geological setting

Whole-rock powder, glass, and mineral separates were analysed from pre-historic Plinian eruptions of Mt. Somma-Vesuvius (Campanian Potassic Volcanic Province) in Southern Italy. Volcanic activity of that area is documented at least for the last 250 ka (Guest et al. 2003), and the magmas are characterized by their silica-undersaturated high alkaline geochemistry (Fig. 2).

Mt. Somma-Vesuvius formed after the great Campanian Ignimbrite Caldera-forming eruption (Orsi et al. 1996) that occurred at the nearby Phlegraean Fields 39 ka ago (De Vivo et al. 2001). Since ca. 20 ka ago, after the formation of the Mt. Somma volcano, the activity at Vesuvius has been characterized by Plinian (e.g. Mercato, Avellino, Pompei) and sub-Plinian (e.g. Pollena and 1631 A.D.) eruptions, which are followed by long periods of quiescence, or by periods of semi-persistent activity (Santacroce 1983). Three magmatic periods have been recognized in the last 20 ka (Santacroce 1983): (1) the first period (~20–9 ka), preceding the Plinian Mercato eruption, is characterized by slightly undersaturated K-basalt to trachyte; the second period (9–2 ka) from the Mercato to Pompei eruptions is characterized by silica-undersaturated magma ranging in composition from tephrite to phonolite; the third period (2 ka–1944 A.D.) is characterized by magma composition ranging from leucititic tephrite to phonolite and mostly as lava flows and strombolian eruptions.

The genesis of the Vesuvian silica-undersaturated K-alkaline magma is still a matter of debate. Previous studies discussed a subduction-related source for Mt. Somma-Vesuvius magmas (e.g. Civetta et al. 1978; Paone 2004, D'Antonio et al. 2007), involving the release of fluids and sediment melts into a fertile asthenosphere during the latest stage of west-directed Apennine subduction of the Adrian plate and the north-west subduction of the Ionian sea floor (Peccerillo 1999). In an alternative view, Lavecchia and Stoppa (1996) proposed an upwelling mantle plume, or possibly a combination of both: upwelling mantle

within a slab window, which leads to a combination of decompression and fluid-induced melting.

Available mineralogical, geochemical and isotopic and geophysical data, (e.g. Civetta et al. 2004; Lima et al. 2003; Zollo et al. 1996), show that the Vesuvius magmatic system is characterized by a ''deep'' reservoir, where mantle-derived melts ascend, stagnate, differentiate, and are contaminated by continental crust (Civetta et al. 2004). A complex system of magma reservoirs extends from the top at 4–6 km down to 15–30 km depth (De Natale et al. 2006). From the ''deep'' reservoirs, magma rises to form shallow magma chambers located at variable depths (4–6 km), hosted within Mesozoic carbonates, where they undergo differentiation, recharge, and mixing before final eruption (e.g., Civetta et al. 1991; Cioni et al. 1998). The shallow reservoir developed from time to time compositional stratification such as documented in the Avellino or Pompei eruptions (e.g. Civetta et al. 1991; Cioni et al. 1995).

We studied whole-rock, glass, single garnet, pyroxene, and amphiboles from a sample collected from the basal fall deposit of the phonolitic Mercato tephra (Member A) and from the phonolitic white pumice fall deposit of Avellino 3. The eruption sequence (Fig. 3) of these pumice deposits is described in detail by Aulinas et al. (2007) and Civetta et al. (1991). Mercato, Avellino 3, and Avellino 7 pumices are different in their degree of differentiation (see Fig. 2) and have distinct strontium isotope compositions (Table 4).

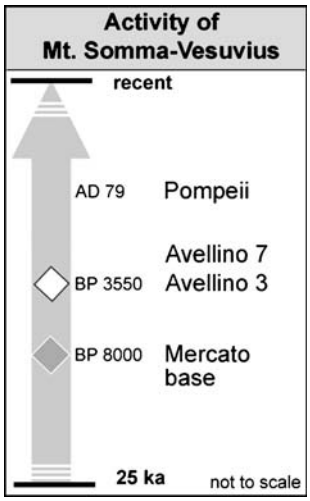

Fig. 3 Stratigraphy of the pre-historic Plinian eruptions Avellino and Mercato of Mt. Somma-Vesuvius. Ages are taken from Cioni et al. (1999b) and Somma et al. (2001, and references herein). A detailed description of the pumice sequences of Avellino and Mercato is given by Cioni et al. (1999b). Legend see Fig. 2

Mercato (CaO = 1.53 wt%) and Avellino 3 (CaO = 2.00 wt%) show a higher degree of differentiation than Avellino 7 phonolite (CaO = 7.82 wt%). The Sr-isotope composition of Avellino 7 whole rock (0.70769) is higher than for Avellino 3 (0.70729) and Mercato (0.70725). On the basis of the chemical and isotope similarity between Mercato phonolite and Avellino first erupted phonolite, and the differences between these and the last erupted Avellino 7 tephritic phonolite. It was suggested that these eruptions tapped a large zoned magma chamber, which is characterized by a phonolite top overlying a tephriphonolite layer (Aulinas et al. 2007). In their model, the zoned reservoir was formed from repeated arrivals of high-T (>1,200°C) isotopically distinct magma batches with subsequent mixing and differentiation.

Analytical methods

Major- and trace elements and oxygen isotopes were measured on whole-rock, glass, and mineral separates of Mercato and Avellino pumices by X-ray fluorescence analysis, inductively coupled plasma mass spectrometry (ICPMS), Laser ablation ICPMS, thermal ionization mass spectrometry, Laser fluorination gas-mass spectrometry and electron microprobe at the ''Geowissenschaftlichen Zentrum'' of the University of Göttingen.

About 1 kg of Mercato and Avellino 3 pumice was leached for 10 days in distilled water changing water daily, crushed and ground to powder in an agate mill. Each sample of 1 g was converted into a glass fusion disk for XRF analysis. Major element analyses were performed on a PHILIPS PW 1460 X-Ray spectrometer following the operation conditions of Hartmann (1994). International standards (JA2 andesite, JB3) were analysed together with samples, the precision for major elements is estimated at <1% (except FeO and Na_2O = 2%) and for trace elements at <5% with abundances >20–30 ppm (Dorendorf et al. 2000).

About 0.1 g of glass and phenocrysts of Mercato and Avellino pumice was separated by hand picking from a crushed sample. About 0.1 g of the whole-rock powder, the glass, and the phenocryst separates were digested in HF/HNO_3 and dried down three times with HNO_3 for ICPMS (Perkin Elmer ELAN DRC II) measurements. As an internal standard we used Ge, Rh, In, and Re and obtained analyses of international standards (JA-2, andesite from the Geological Survey of Japan; BHVO-1, Hawaiian basalt from the US Geological Survey) during measurement pro-

cedure. Analytical uncertainty for trace elements is ±10%.

In situ rare earth element measurements were performed by LA-ICPMS (Perkin Elmer ELAN DRC II) on polished mineral separates of grandites and pyroxenes, using an ArF-Excimer laser at 193 nm. Samples were ablated with a pulse energy of 0.2 mJ at 10 Hz. Spot diameters range from 10 to 60 μm. ^{43}Ca was used as an internal standard, based on concentration determined by electron microprobe. The calibration was monitored and accuracy estimated by repeated analyses of an Al–Ca-rich standard glass (NBS 610) of the National Institute of Science and Technology (NIST), doped with 61 elements at the 500 ppm level (Rocholl et al. 1997). Analytical uncertainties are ±10% (2σ) for rare earth elements. The detection limit ranges between 0.11 (for Lu) and 0.30 ppm (for Nd) (5σ of blank analysis on 60 μm laser spot).

Oxygen isotopes were measured on individual garnet and feldspar grains with the CO_2-laser fluorination technique by reacting the samples under a F_2 gas atmosphere. Purified oxygen gas was transferred into a Finnigan Delta Plus Mass Spectrometer via a zeolite molecular sieve. All data are given in the standard δ-notation, as ‰-deviation from SMOW. During the course of analysis, a laboratory standard (UWG-2 garnet; $\delta^{18}O_{SMOW}$ = 5.8‰; Valley et al. 1995) was measured twice a day and gave an average value of 5.8 ± 0.2‰ (2σ).

Strontium isotopes were determined by thermal ionization mass spectrometer (Finnigan MAT 262 RPQ II+) after HF/HNO_3 total digestion in Teflon beakers and column separation. Sr-isotopes were corrected for mass fractionation to $^{86}Sr/^{88}Sr$ = 0.1194 and normalized to values for NBS987 (0.710245). Repeated analyses of standard NBS987 over the period of this study gave a mean value for $^{87}Sr/^{86}Sr$ = 0.710249 ± 0.000012 (2σ). Analytical uncertainty of $^{87}Sr/^{86}Sr$-ratios for samples is given by ±0.00001.

Major element analyses on grandites and pyroxenes were obtained by electron microprobe (JEOL JXA 8900 RL). Quantitative WDX electron microprobe analyses were conducted at an accelerating voltage of 15 kV and a beam current of 20 nA using various natural and synthetic standards.

Results

Major elements of Avellino and Mercato grandites

Garnets from Avellino 3 and Mercato (Table 2) are both grandite solid-solutions between the iron-rich end-member Ti-andradite ($Ca_3(Fe^{3+},Ti)_2[(Si,Al,Fe^{3+})_3O_{12}]$) and the aluminium-rich end-member grossularite ($Ca_3Al_2[(Si_3O_{12})]$. Andradite fractions were calculated assuming that the fraction of uvarovite (Cr-exchange on octahedral position) is negligible. Fe^{3+} was calculated from the micro probe data assuming a non-hydrated ideal stoichiometric composition. The titanium endmembers schorlomite ($Ca_3Ti_2[Fe^{3+}{}_2SiO_{12}]$), morimotoite ($Ca_3Fe^{2+}Ti_2[Si_3O_{12}]$) and the zirconium-bearing kimzeyite ($Ca_3Zr_2[Al_2SiO_{12}]$) were also taken into account. For simplification, however, all calculated Fe^{3+} is regarded as ''andradite-component'' (Table 3).

Garnets from Mercato are Ti- and Fe-rich andradites, unzoned and have abundant sanidine and some minor inclusions of clinopyroxene, titanite, apatite and pyrrhotite (Fig. 4). The grandites from Mercato pumice show only a small variation in their Al–Fe-content between $Gro_{31}And_{69}$ and $Gro_{33}And_{67}$. By contrast, Avellino 3 grandites show a wide range in their Al–Fe-contents between $Gro_{30}And_{70}$ and $Gro_{40}And_{60}$. Grandites from Avellino 3 pumice are Ti- and Al-rich andradites characterized by a complex oscillatory zoning and contain noticeably more mineral inclusions than Mercato garnets. Mineral inclusions in Avellino 3 garnets are sanidine, sphene, apatite, clinopyroxene and Fe-sulphides (Figs. 5, 6).

On the basis of the molar (Mg/(Mg+Fe)) ratio of Avellino grandites between 0.004 and 0.08 and a relatively high (Mg/(Mg+Fe)) ratio for the coexisting Avellino melt (0.08) (i.e. grandites are more Fe-rich than the coexisting melt), it is suggested that the grandites crystallized at a temperature below 950°C (Green 1977). Such low crystallization temperature for Avellino and Mercato grandites has also been reported by Scaillet and Pichavant (2004), who demonstrated that by crystallisation experiments a stability field for grandites in Mercato and Avellino melts at a temperature below 800°C and a pressure of 2 kb.

Trace elements

Mercato grandites are homogeneous in their rare earth element distribution, which was expected because of the unzoned major element composition (Table 2b). The grandites show typical chondrite-normalized REE patterns with HREE-enrichment with respect to the LREE (Fig. 10a). In contrast, the garnets of Avellino 3 are highly variable in chondrite-normalized HREE and show lower chondrite-normalized HREE than Mercato (Fig. 10a–d). Avellino patterns for REE are thus quite distinct from those of Mercato garnets and rather atypical in their variable and large HREE depletion.

Table 2 Major and trace elements of (a) whole-rock and (b) garnet of Mercato and Avellino eruption (Somma-Vesuvius volcanic complex, South Italy)

(a) Whole-rock

Sample type	Whole-rock	Glass	Whole-rock	Glass	Whole-rock
Origin of sample	Mercato	Mercato	Avellino 3	Avellino 3	Avellino 7
Age of eruption (ka)	8.1	8.1	3.7	3.7	3.7
In wt%					
SiO_2^{XRF}	56.4		54.5		52.4
TiO_2^{XRF}	0.10		0.13		0.46
$Al_2O_3^{XRF}$	20.4		22.4		18.0
FeO^{XRF}	1.98		1.90		4.54
MnO^{XRF}	0.18		0.12		0.13
MgO^{XRF}	0.08		0.16		3.05
CaO^{XRF}	1.53		2.0		7.82
Na_2O^{XRF}	8.06		8.31		4.82
K_2O^{XRF}	6.59		7.31		6.21
$P_2O_5^{XRF}$	0.01		0.03		0.29
wt. % total	95.33		96.82		97.72
In ppm					
Y^{XRF}	8.54	16.4	2.26	3.02	13.3
Zr^{XRF}	770	1086	657	858	770
La^{ICP-MS}	72	82	46	56	60
Ce^{ICP-MS}	148	150	110	110	121
Pr^{ICP-MS}	11.2	15.2	7.51	9.9	11.4
Nd^{ICP-MS}	30.3	44.4	17.5	23.7	36.5
Sm^{ICP-MS}	3.32	4.98	1.29	1.62	5.62
Eu^{ICP-MS}	0.37	0.55	0.23	0.25	1.34
Gd^{ICP-MS}	3.68		2.00		5.70
Tb^{ICP-MS}	0.31	0.46	0.13	0.10	0.60
Dy^{ICP-MS}	1.35	2.15	0.45	0.36	2.77
Ho^{ICP-MS}	0.27	0.42	0.08	0.08	0.50
Er^{ICP-MS}	0.92	1.44	0.28	0.23	1.43
Tm^{ICP-MS}	0.14	0.23	0.04	0.03	0.18
Yb^{ICP-MS}	1.03	1.72	0.23	0.20	1.17
Lu^{ICP-MS}	0.18	0.31	0.04	0.03	0.18
Th^{ICP-MS}	92.1	105	84.9	87.5	43.5
U^{ICP-MS}	37.4	46.9	35.9	37.5	16.2

(b) Garnet of Mercato and Avellino eruption

Sample type	Garnet											
Origin of sample	Mercato											
Age of eruption (ka)	8.1											
No. of zone	1.1	1.3	1.4	2.1	2.2	2.3	3.1	3.2	3.3	3.4	3.5	3.6
SiO_2^{EMS}	34.9	34.9	34.9	34.7	34.7	34.7	34.7	34.7	34.7	34.7	34.7	34.7
TiO_2^{EMS}	3.06	3.06	3.06	2.91	2.91	2.91	3.06	3.06	3.06	3.06	3.06	3.06
$Al_2O_3^{EMS}$	5.86	5.86	5.86	5.76	5.76	5.76	5.83	5.83	5.83	5.83	5.83	5.83
FeO^{EMS}	20.5	20.5	20.5	20.5	20.5	20.5	20.5	20.5	20.5	20.5	20.5	20.5
MnO^{EMS}	1.88	1.88	1.88	1.99	1.99	1.99	1.86	1.86	1.86	1.86	1.86	1.86
MgO^{EMS}	0.25	0.25	0.25	0.28	0.28	0.28	0.25	0.25	0.25	0.25	0.25	0.25
CaO^{EMS}	31.2	31.2	31.2	31.4	31.4	31.4	31.5	31.5	31.5	31.5	31.5	31.5
Na_2O^{EMS}	BD	BD	BD	BD	BD	BD	BD	BD	BD	BD	BD	BD
K_2O^{EMS}	BD	BD	BD	BD	BD	BD	BD	BD	BD	BD	BD	BD
wt. % total	98.36	98.36	98.36	98.23	98.23	98.23	98.29	98.29	98.29	98.29	98.29	98.29
Grossular (mol%)	32%	32%	32%	31%	31%	31%	32%	32%	32%	32%	32%	32%
Andradit (mol%)	68%	68%	68%	69%	69%	69%	68%	68%	68%	68%	68%	68%
$La^{La-ICP-MS}$	39.1	43.1	56.6	45.6	43.2	43.1	41.1	42.7	43.7	42.5	43.3	43.2
$Ce^{La-ICP-MS}$	281	320	359	327	322	306	309	310	320	325	325	330
$Pr^{La-ICP-MS}$	81.3	86.7	88.8	90.3	88.1	78.6	86.6	87.0	87.3	87.6	89.6	89.7
$Nd^{La-ICP-MS}$	628	661	646	694	668	609	670	660	671	662	688	679
$Sm^{La-ICP-MS}$	225	243	238	259	251	223	246	245	244	246	245	246
$Eu^{La-ICP-MS}$	33.0	36.8	36.9	38.9	37.1	34.5	35.1	35.3	36.2	34.8	36.1	35.7
$Gd^{La-ICP-MS}$	205	222	212	237	228	195	206	214	216	209	212	214
$Tb^{La-ICP-MS}$	35.6	37.5	36.1	40.4	38.6	32.6	33.5	34.9	35.5	34.3	34.5	34.9
$Dy^{La-ICP-MS}$	223	237	227	257	241	203	202	210	211	210	208	214
$Ho^{La-ICP-MS}$	50.0	53.1	51.3	57.9	55.1	45.7	43.6	46.2	46.1	45.4	45.5	47.1
$Er^{La-ICP-MS}$	156	169	163	187	172	143	137	145	145	142	145	148
$Tm^{La-ICP-MS}$	25.7	27.1	26.0	29.8	27.5	22.9	22.0	23.2	23.7	22.9	23.1	23.4
$Yb^{La-ICP-MS}$	183	199	187	213	204	167	170	172	175	169	171	174
$Lu^{La-ICP-MS}$	26.9	28.3	27.3	31.0	29.1	23.8	24.7	25.7	26.3	24.5	25.2	26.0
$Th^{La-ICP-MS}$	27.4	26.5	30.9	28.0	25.7	23.0	25.9	26.8	26.1	25.5	26.0	27.6
$U^{La-ICP-MS}$	30.9	29.8	31.9	30.9	29.7	34.7	31.2	31.6	30.1	29.4	30.6	34.7

Table 2 continued

Sample type	Garnet											
Origin of sample	Mercato											
Age of eruption (ka)												
No. of zone	4.3	4.5	4.6	5.1	5.2	5.3	5.4	7.1	7.2	7.3	8.1	8.2
SiO_2^{EMS}	34.8	34.8	34.8	34.9	34.9	34.9	34.9	35.0	35.0	35.0	35.0	35.0
TiO_2^{EMS}	2.72	2.72	2.72	2.72	2.72	2.72	2.72	2.74	2.74	2.74	2.88	2.88
$Al_2O_3^{EMS}$	5.81	5.81	5.81	5.86	5.86	5.86	5.86	5.86	5.86	5.86	5.99	5.99
FeO^{EMS}	20.5	20.5	20.5	20.6	20.6	20.6	20.6	20.5	20.5	20.5	20.3	20.3
MnO^{EMS}	1.91	1.91	1.91	1.89	1.89	1.89	1.89	1.99	1.99	1.99	1.95	1.95
MgO^{EMS}	0.24	0.24	0.24	0.24	0.24	0.24	0.24	0.24	0.24	0.24	0.27	0.27
CaO^{EMS}	31.2	31.2	31.2	31.7	31.7	31.7	31.7	31.4	31.4	31.4	31.3	31.3
Na_2O^{EMS}	BD	BD	BD	BD	BD	BD	BD	BD	BD	BD	BD	BD
K_2O^{EMS}	BD	BD	BD	BD	BD	BD	BD	BD	BD	BD	BD	BD
wt. % total	97.77	97.77	97.77	98.57	98.57	98.57	98.57	98.31	98.31	98.31	98.42	98.42
Grossular (mol%)	31%	31%	31%	31%	31%	31%	31%	32%	32%	32%	33%	33%
Andradit (mol%)	69%	69%	69%	69%	69%	69%	69%	68%	68%	68%	67%	67%
$La^{La\text{-}ICP\text{-}MS}$	40.4	38.9	44.0	46.8	37.3	39.8	41.0	38.8	37.5	38.7	36.7	38.7
$Ce^{La\text{-}ICP\text{-}MS}$	304	303	343	376	294	293	306	286	298	282	275	282
$Pr^{La\text{-}ICP\text{-}MS}$	84.5	79.8	89.3	97.5	74.6	81.9	84.2	79.1	83.5	78.6	80.5	78.6
$Nd^{La\text{-}ICP\text{-}MS}$	647	590	667	895	558	625	641	603	626	601	592	601
$Sm^{La\text{-}ICP\text{-}MS}$	242	224	245	243	189	235	243	219	215	231	224	231
$Eu^{La\text{-}ICP\text{-}MS}$	36.4	35.2	37.3	36.3	31.3	35.4	37.1	34.3	32.9	33.4	33.8	33.4
$Gd^{La\text{-}ICP\text{-}MS}$	215	199	222	263	196	209	222	207	193	212	216	212
$Tb^{La\text{-}ICP\text{-}MS}$	37.0	33.6	36.4	45.2	33.6	36.1	38.5	35.9	33.3	37.2	37.8	37.2
$Dy^{La\text{-}ICP\text{-}MS}$	228	209	230	259	193	227	244	225	205	237	245	237
$Ho^{La\text{-}ICP\text{-}MS}$	51.5	47.1	51.8	59.0	46.4	51.0	55.4	49.6	45.2	54.5	55.7	54.5
$Er^{La\text{-}ICP\text{-}MS}$	165	150	162	155	148	160	175	147	136	169	172	169
$Tm^{La\text{-}ICP\text{-}MS}$	25.7	24.0	25.9	33.1	21.0	26.0	28.2	24.1	22.5	27.3	28.5	27.3
$Yb^{La\text{-}ICP\text{-}MS}$	190	175	190	203	166	190	207	176	165	201	209	201
$Lu^{La\text{-}ICP\text{-}MS}$	27.7	25.0	27.2	24.7	22.2	27.3	29.7	26.3	23.1	29.7	30.3	29.7
$Th^{La\text{-}ICP\text{-}MS}$	23.1	23.1	24.8	34.7	30.7	23.6	25.2	25.8	27.0	27.8	27.1	27.8
$U^{La\text{-}ICP\text{-}MS}$	27.2	33.4	32.4	38.4	31.2	26.1	28.7	29.4	31.1	31.7	33.5	31.7

Sample type	Garnet											
Origin of sample	Mercato					Avellino 3						
Age of eruption (ka)						3.7						
No. of zone	8.4	10.1	10.2	11.1	11.2	11.3	2.1	2.2	2.3	2.6	2.7	2.8
SiO_2^{EMS}	35.0	35.1	35.1	34.6	34.6	34.6	35.4	35.3	35.3	35.3	35.3	35.3
TiO_2^{EMS}	2.88	2.75	2.75	2.98	2.98	2.98	1.80	1.81	1.81	1.81	1.81	1.81
$Al_2O_3^{EMS}$	5.99	5.88	5.88	5.69	5.69	5.69	5.83	7.62	7.62	7.62	7.62	7.62
FeO^{EMS}	20.3	20.7	20.7	20.6	20.6	20.6	20.8	19.0	19.0	19.0	19.0	19.0
MnO^{EMS}	1.95	2.01	2.01	1.90	1.90	1.90	1.55	1.74	1.74	1.74	1.74	1.74
MgO^{EMS}	0.27	0.26	0.26	0.27	0.27	0.27	0.12	0.15	0.15	0.15	0.15	0.15
CaO^{EMS}	31.3	31.6	31.6	31.8	31.8	31.8	32.9	32.1	32.1	32.1	32.1	32.1
Na_2O^{EMS}	BD	BD	BD	BD	BD	BD	BD	BD	BD	BD	BD	BD
K_2O^{EMS}	BD	BD	BD	BD	BD	BD	BD	BD	BD	BD	BD	BD
wt. % total	98.42	98.90	98.90	98.42	98.42	98.42	98.74	98.10	98.10	98.10	98.10	98.10
Grossular (mol%)	33%	31%	31%	33%	33%	33%	30%	38%	38%	38%	38%	38%
Andradit (mol%)	67%	69%	69%	67%	67%	67%	70%	62%	62%	62%	62%	62%
$La^{La\text{-}ICP\text{-}MS}$	56.2	42.8	39.8	45.6	39.9	41.9	19.6	23.4	25.8	28.1	35.6	32.0
$Ce^{La\text{-}ICP\text{-}MS}$	372	311	298	332	296	316	137	199	218	220	264	277
$Pr^{La\text{-}ICP\text{-}MS}$	88.5	85.9	82.8	91.5	82.8	86.2	35.1	53.0	56.7	56.8	65.7	68.9
$Nd^{La\text{-}ICP\text{-}MS}$	649	655	637	688	634	658	181	322	331	336	385	409
$Sm^{La\text{-}ICP\text{-}MS}$	245	248	244	250	242	248	18.8	43.2	40.2	39.9	52.9	47.6
$Eu^{La\text{-}ICP\text{-}MS}$	37.2	37.0	37.4	37.6	36.2	37.2	1.54	3.55	3.42	3.51	5.24	3.97
$Gd^{La\text{-}ICP\text{-}MS}$	229	231	230	224	223	222	3.53	7.97	7.86	7.46	10.8	7.89
$Tb^{La\text{-}ICP\text{-}MS}$	40.1	39.2	39.2	37.0	37.7	38.1	0.27	0.46	0.46	0.50	0.73	0.45
$Dy^{La\text{-}ICP\text{-}MS}$	254	246	248	230	238	239	0.42	1.04	1.17	1.06	2.07	1.34
$Ho^{La\text{-}ICP\text{-}MS}$	57.7	55.2	57.2	51.6	55.4	54.2	0.07	0.16	0.11	0.13	0.30	0.19
$Er^{La\text{-}ICP\text{-}MS}$	183	178	182	165	175	172	0.27	0.24	0.45	0.31	0.73	0.63
$Tm^{La\text{-}ICP\text{-}MS}$	29.4	28.6	29.3	26.0	27.7	27.2	BD	0.04	0.06	0.05	0.11	0.04
$Yb^{La\text{-}ICP\text{-}MS}$	215	206	209	191	203	198	0.04	0.69	0.35	0.41	0.86	0.27
$Lu^{La\text{-}ICP\text{-}MS}$	30.9	29.9	30.8	27.8	28.8	28.6	0.03	0.05	0.03	0.06	0.16	0.06
$Th^{La\text{-}ICP\text{-}MS}$	31.1	26.5	22.3	25.9	20.9	22.3	21.3	15.6	16.2	13.3	13.4	18.1
$U^{La\text{-}ICP\text{-}MS}$	37.1	30.7	25.8	30.0	24.5	27.0	11.4	24.2	22.5	19.5	18.5	26.0

Table 2 continued

Sample type	Garnet											
Origin of sample	Avellino 3											
Age of eruption (ka)												
No. of zone	2.9	2.10	2.11	3.1	3.2	3.3	3.4	3.5	3.6	3.7	3.8	4.2
SiO_2^{EMS}	35.4	35.4	35.3	35.6	35.4	35.6	35.4	35.6	35.6	35.6	35.6	35.0
TiO_2^{EMS}	1.80	1.80	1.81	1.63	2.61	1.63	2.61	1.63	1.63	1.63	1.63	3.83
$Al_2O_3^{EMS}$	5.83	5.83	7.62	6.19	7.25	6.19	7.25	6.19	6.19	6.19	6.19	7.42
FeO^{EMS}	20.8	20.8	19.0	20.3	19.2	20.3	19.2	20.3	20.3	20.3	20.3	18.7
MnO^{EMS}	1.55	1.55	1.74	2.03	1.44	2.03	1.44	2.03	2.03	2.03	2.03	0.88
MgO^{EMS}	0.12	0.12	0.15	0.09	0.26	0.09	0.26	0.09	0.09	0.09	0.09	0.35
CaO^{EMS}	32.9	32.9	32.1	31.7	31.5	31.7	31.5	31.7	31.7	31.7	31.7	32.6
Na_2O^{EMS}	BD	BD	BD	BD	BD	BD	BD	BD	BD	BD	BD	BD
K_2O^{EMS}	BD	BD	BD	BD	BD	BD	BD	BD	BD	BD	BD	BD
wt. % total	98.74	98.74	98.10	97.84	98.06	97.84	98.06	97.84	97.84	97.84	97.84	99.19
Grossular (mol%)	30%	30%	38%	33%	39%	33%	39%	33%	33%	33%	33%	40%
Andradit (mol%)	70%	70%	62%	67%	61%	67%	61%	67%	67%	67%	67%	60%
$La^{La\text{-}ICP\text{-}MS}$	17.7	24.4	49.4	10.7	16.7	11.1	21.2	18.3	17.5	11.4	11.3	51.4
$Ce^{La\text{-}ICP\text{-}MS}$	172	181	288	118	134	126	160	173	173	128	132	270
$Pr^{La\text{-}ICP\text{-}MS}$	41.8	37.1	64.8	30.9	37.2	32.7	41.5	43.1	42.6	30.5	30.6	58.1
$Nd^{La\text{-}ICP\text{-}MS}$	231	138	383	139	264	143	251	192	199	124	124	348
$Sm^{La\text{-}ICP\text{-}MS}$	21.3	7.26	51.6	8.34	75.6	11.1	50.0	11.3	11.4	8.59	8.34	92.2
$Eu^{La\text{-}ICP\text{-}MS}$	1.60	0.50	5.15	1.33	10.9	1.53	7.51	1.69	1.48	1.45	1.19	21.7
$Gd^{La\text{-}ICP\text{-}MS}$	2.55	1.17	11.0	1.62	41.0	2.43	22.13	1.56	1.60	2.00	1.80	72.4
$Tb^{La\text{-}ICP\text{-}MS}$	0.11	BD	0.69	0.11	4.87	0.20	2.37	0.11	0.08	0.12	0.12	11.3
$Dy^{La\text{-}ICP\text{-}MS}$	0.19	0.15	1.60	0.37	23.2	0.68	10.26	0.28	0.17	0.49	0.32	60.6
$Ho^{La\text{-}ICP\text{-}MS}$	0.03	0.04	0.21	0.06	3.86	0.10	1.65	0.02	0.03	0.05	0.03	12.2
$Er^{La\text{-}ICP\text{-}MS}$	BD	0.06	0.60	0.10	11.2	0.26	5.33	0.09	0.06	0.13	0.10	33.3
$Tm^{La\text{-}ICP\text{-}MS}$	BD	BD	0.07	0.02	1.66	0.02	0.83	0.00	0.01	0.02	0.02	4.81
$Yb^{La\text{-}ICP\text{-}MS}$	0.03	BD	0.64	0.13	14.8	0.30	6.30	0.07	0.13	0.15	0.10	34.0
$Lu^{La\text{-}ICP\text{-}MS}$	0.01	BD	0.15	0.02	2.49	0.04	1.05	0.00	0.00	0.01	0.01	4.79
$Th^{La\text{-}ICP\text{-}MS}$	14.1	18.3	21.5	21.9	22.7	18.8	23.3	17.1	17.8	18.9	18.3	29.1
$U^{La\text{-}ICP\text{-}MS}$	16.9	15.3	22.0	2.8	19.9	2.6	7.4	5.4	4.7	4.2	4.2	21.2

Sample type	Garnet							
Origin of sample	Avellino 3							
Age of eruption (ka)								
No. of zone	4.3	4.5	4.6	5.2	5.3	5.4	5.5	5.6
SiO_2^{EMS}	35.4	35.4	35.4	35.5	35.5	35.5	35.6	35.6
TiO_2^{EMS}	3.02	3.02	3.02	1.88	1.88	1.88	1.88	1.88
$Al_2O_3^{EMS}$	8.56	8.56	8.56	7.79	7.79	7.79	7.73	7.73
FeO^{EMS}	17.2	17.2	17.2	18.8	18.8	18.8	19.0	19.0
MnO^{EMS}	1.38	1.38	1.38	1.67	1.67	1.67	1.68	1.68
MgO^{EMS}	0.25	0.25	0.25	0.15	0.15	0.15	0.15	0.15
CaO^{EMS}	32.3	32.3	32.3	32.2	32.2	32.2	31.6	31.6
Na_2O^{EMS}	BD	BD	BD	BD	BD	BD	BD	BD
K_2O^{EMS}	BD	BD	BD	BD	BD	BD	BD	BD
wt. % total	98.52	98.52	98.52	98.33	98.33	98.33	98.03	98.03
Grossular (mol%)	45%	45%	45%	39%	39%	39%	40%	40%
Andradit (mol%)	55%	55%	55%	61%	61%	61%	60%	60%
$La^{La\text{-}ICP\text{-}MS}$	18.6	23.2	38.8	49.4	71.2	37.9	33.8	35.0
$Ce^{La\text{-}ICP\text{-}MS}$	167	171	202	292	321	289	256	263
$Pr^{La\text{-}ICP\text{-}MS}$	48.6	47.3	49.2	67.1	66.4	66.0	65.8	65.9
$Nd^{La\text{-}ICP\text{-}MS}$	319	309	308	380	374	388	386	386
$Sm^{La\text{-}ICP\text{-}MS}$	53.0	57.3	48.8	60.5	50.9	52.4	46.4	43.3
$Eu^{La\text{-}ICP\text{-}MS}$	7.50	8.36	5.98	7.67	5.79	5.09	3.80	3.68
$Gd^{La\text{-}ICP\text{-}MS}$	23.9	28.6	21.1	18.6	13.9	11.9	8.53	8.36
$Tb^{La\text{-}ICP\text{-}MS}$	3.15	3.90	2.60	1.76	1.05	0.80	0.42	0.48
$Dy^{La\text{-}ICP\text{-}MS}$	16.9	21.14	13.25	6.70	3.62	2.37	1.26	1.15
$Ho^{La\text{-}ICP\text{-}MS}$	3.48	4.14	2.42	1.15	0.41	0.26	0.15	0.14
$Er^{La\text{-}ICP\text{-}MS}$	9.51	12.2	6.83	3.17	1.22	0.70	0.29	0.33
$Tm^{La\text{-}ICP\text{-}MS}$	1.49	1.90	1.05	0.41	0.18	0.12	0.04	0.04
$Yb^{La\text{-}ICP\text{-}MS}$	9.80	12.4	7.97	4.05	1.72	0.94	0.44	0.53
$Lu^{La\text{-}ICP\text{-}MS}$	1.57	1.82	1.10	0.60	0.37	0.22	0.11	0.06
$Th^{La\text{-}ICP\text{-}MS}$	16.0	16.4	33.9	18.3	28.4	14.0	18.1	18.9
$U^{La\text{-}ICP\text{-}MS}$	27.0	26.0	26.6	15.6	16.9	20.1	21.9	22.0

XRF X-ray fluorescence, *ICP-MS* inductively coupled plasma mass spectrometry, *La-ICP-MS* laser ablation ICPMS, *EMS* electron microprobe, *BD* below detection limit

Table 3 Major element composition analysed by electron microprobe for pyroxenes and amphiboles of Avellino 3

	Pyroxene 1 Avellino 3	Pyroxene 1 Avellino 3	Pyroxene 1 Avellino 3	Pyroxene 2 Avellino 3	Pyroxene 2 Avellino 3	Pyroxene 3 Avellino 3	Pyroxene 3 Avellino 3	Amphibole Avellino 3
In wt%								
SiO_2	53.5			48.7		45.4		35.5
TiO_2	0.30			0.83		1.3		1.4
Al_2O_3	1.15			5.23		8.2		13.4
FeO	2.85			6.14		9.2		27.9
MnO	BD			0.1		BD		1.7
MgO	17.3			13.7		11.0		2.1
CaO	24.4			24.7		23.9		11.0
Na_2O	BD			BD		BD		2.10
K_2O	BD			BD		BD		2.37
wt% total	99.4			99.4		99.0		97.5
In ppm								
La	3.9	3.8	3.9	11	11	88	48	82
Ce	12	13	13	32	37	172	100	233
Pr	2.3	2.1	2.3	5.8	6.5	22	13	32
Nd	14	14	14	36	35	101	56	112
Sm	4.6	4.0	4.6	10.2	10.1	23	11	5.9
Eu	1.1	1.1	1.1	2.5	2.5	5.3	2.4	0.44
Gd	3.5	3.8	3.7	7.6	7.7	17.0	7.5	1.3
Tb	0.50	0.46	0.46	1.0	0.9	2.0	0.9	0.10
Dy	2.3	2.2	2.4	5.3	5.1	10	4.5	0.17
Ho	0.34	0.35	0.34	0.9	0.9	1.7	0.8	0.03
Er	0.8	0.7	0.8	2.7	2.1	4.0	1.8	0.06
Tm	0.08	0.09	0.13	0.34	0.28	0.47	0.24	BD
Yb	0.59	0.56	0.49	2.0	1.4	2.9	1.6	0.10
Lu	0.07	0.06	0.09	0.22	0.22	0.40	0.25	BD

BD below detection limit

Oxygen and strontium isotopes

Mercato grandites show $\delta^{18}O_{SMOW}$ -values between 6.8 and 8.5‰, which is lower than the $\delta^{18}O_{SMOW}$-values of their host rocks (9.0 to 9.5‰; Ayuso et al. 1998). Avellino garnets range from 7.1 to 7.9‰ (Table 4). Mercato grandites show the same strontium isotope composition (0.70724 ± 1) as their host-rocks (0.70725 ± 1).

Discussion

First, we discuss whether the garnets from Mercato and Avellino pumice are of magmatic or hydrothermal origin. Indications for a magmatic origin of the garnets are the high fractionated Ce/Yb ratios of Mercato and Avellino phonolites compared to all other volcanic products from Vesuvius (Fig. 7). This indicates that especially Mercato and Avellino 3 melts were affected by significant garnet fractionation, whereas the other eruption products of Mt. Somma-Vesuvius were affected at most by minor garnet removal (Fig. 7). This can be explained by the chemical composition of Mercato and Avellino 3 magma. Both are highly evolved, alkaline silica-undersaturated magmas, which permit the precipitation of a relatively *large* amount of garnet. As mentioned earlier, crystallisation experiments of Scaillet and Pichavant (2004) indicate that garnet crystallisation for Mercato and Avellino melts at low temperatures and pressure and in the absence of calcareous (country) rocks.

Morphology, colour and TiO_2-content of grandites

Skarn-associated and magmatic grandites world-wide both show a large variability in their morphology, colour, zonation style and chemical composition (Naimo et al. 2003; Russell et al. 1999; Smith et al. 2004; Fulignati et al. 2004; Cioni et al. 1995; Table 1). Both can occur zoned or unzoned and have high (>1%) or low (<1%) TiO_2 content (Table 1). Grandites can appear in various colours, but the magmatic variety, produced in alkaline magmas such as trachyte (Ferguson and Edgar 1978), syenite (Turbeville 1993, Lang et al. 1995), nepheline-syenite (Gomes 1969) or phonolite (Amthauer et al. 1977) are generally dark brown or black. The colour of these magmatic grandites is caused by their high quantity of titanium (>1 wt%). In

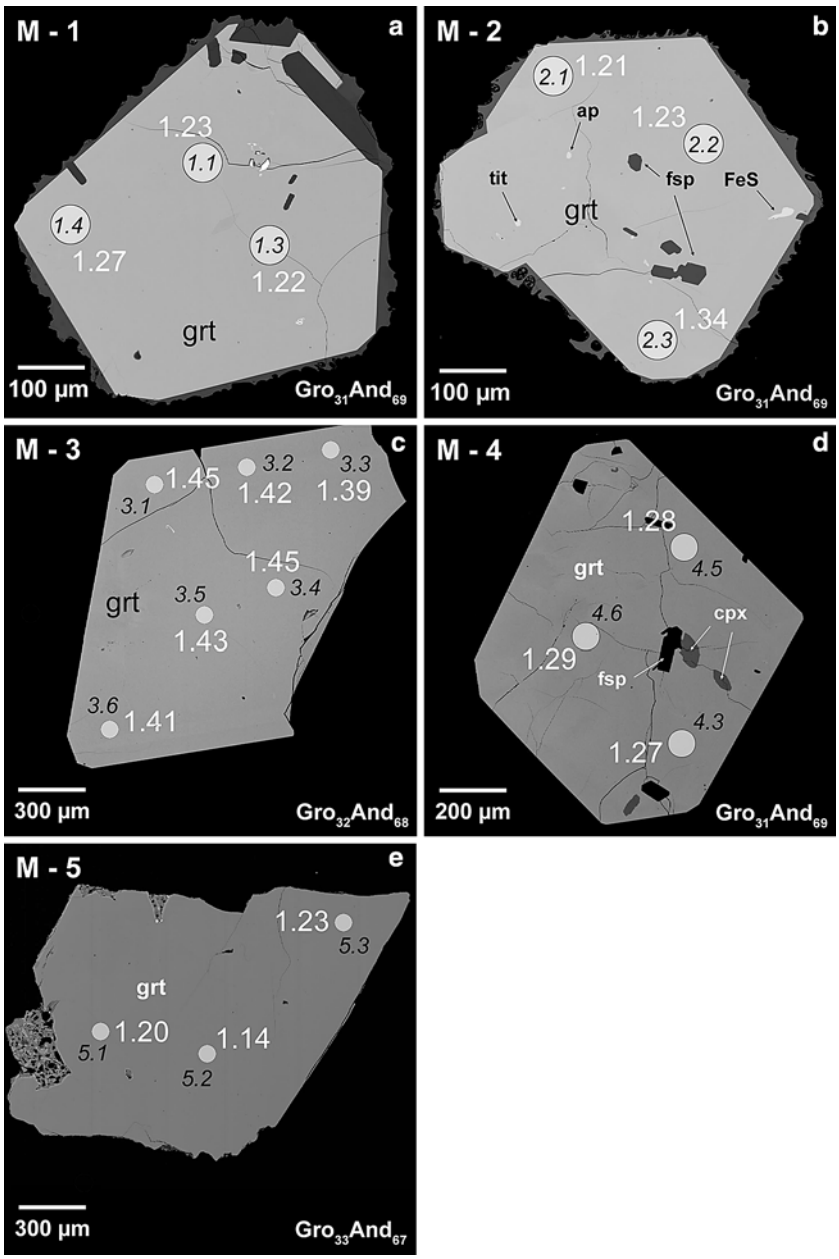

Fig. 4 Back scattered electron (BSE) images performed by EMP from five Mercato grandites (M-1 to M-5). All Mercato grandites are unzoned and homogeneous in their major and trace element concentrations. The position and the size of the spots from selected LA-ICPMS measurements are marked by *white solid circles*. Lab-IDs of the LA-ICPMS measurements given in *black numbers*, Sm/Yb-ratios are written in *white numbers*. *Tit* titanite, *ap* apatite, *grt* garnet, *fsp* feldspar, *cpx* clinopyroxene, *px* pyroxene

contrast, most grandites produced during metasomatic, hydrothermal or metamorphic processes are red, yellow, brown, and green, because of their lower TiO_2 contents. Examples of hydrothermal/metasomatic grandites associated with skarn-forming processes and with low TiO_2 content are found in the Beinn-an-Dubhaich granite aureole at the Isle of Skye/Scotland (Smith et al. 2004) and from Mt. Somma-Vesuvius (Fulignati et al. 2005; Table 1). The low TiO_2-content of skarn-derived grandites reflects the small quantity of TiO_2 in host carbonates. Exceptions are unzoned titanium andradites (TiO_2 = 12.4%) from a skarn deposit of the Northern Red Sea Hill in Sudan (Huggins et al. 1977) and zoned hydrothermal titanian andradites from Galore Creek in the Canadian Cordillera (TiO_2 = 2.0%) (Russell et al. 1999). It follows that the morphology, colour, TiO_2-content, and zonation style of Mercato and Avellino 3 garnets alone cannot be used to distinguish magmatic from skarn-derived garnets.

Isotope composition

Oxygen isotope compositions of Mt. Somma-Vesuvius grandites are useful for distinguishing between a magmatic or metasomatic origin because of their host

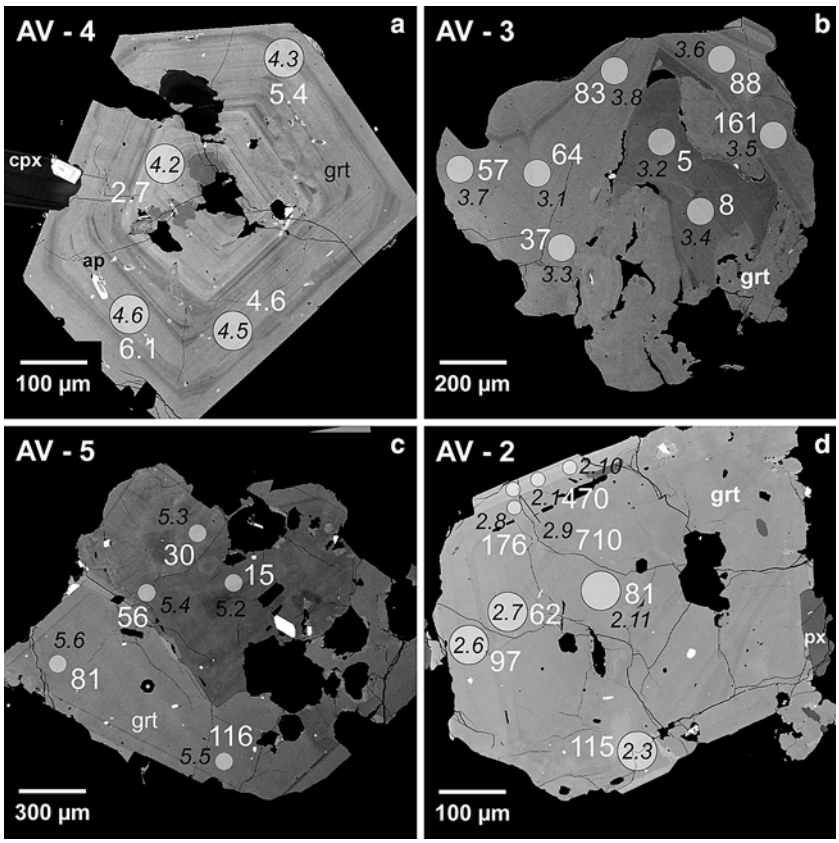

Fig. 5 BSE images of grandites from Avellino 3 pumice (AV-2 to AV-5). All analysed garnets are zoned and heterogeneous in their major- and/or trace elements. For the legend see Fig. 4

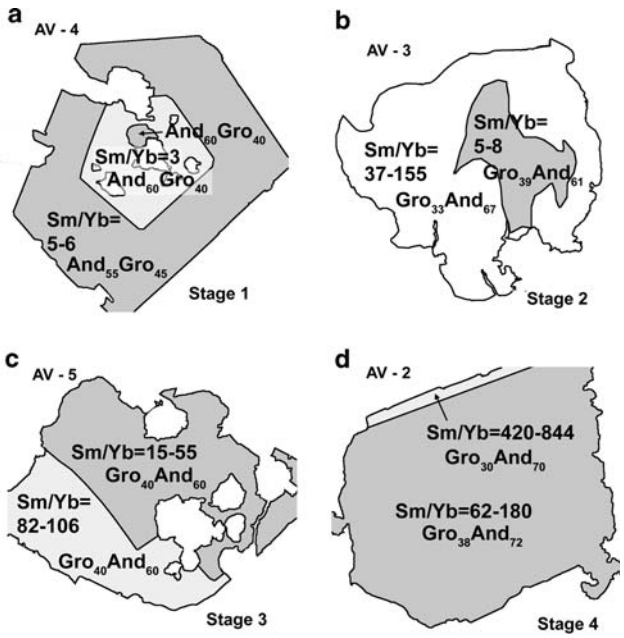

Fig. 6 Schematic illustration of principal zonation patterns with regard to Al (grossularite) and Fe (andradite) and variations in Sm/Yb ratios

melt (Table 4), the magmatic fluids, and the country rocks from which the skarns formed show significantly different $\delta^{18}O_{SMOW}$ values (Fulignati et al. 2005; Gilg et al. 2001). Furthermore, refractory minerals such as garnet or zircon provide a clear record of the $\delta^{18}O_{SMOW}$ values of their host magma or host rock and are not affected by significant oxygen fractionation processes during crystallization or diffusion (Kohn and Valley 1998; Vielzeuf et al. 2005; Lackey et al. 2006). Hence, the skarn-related grandites from Mt. Somma-Vesuvius should have $\delta^{18}O_{SMOW}$ values between the magmatic fluid and the carbonate protolith, based on the following equation:

$$\underset{\text{carbonate}}{3CaCO_3} + \underset{\text{magmatic fluid}}{Fe_2O_3 + 3SiO_2} \rightarrow \underset{\text{andradite}}{Ca_3Fe_2Si_3O_{12}} + 3CO_2 \quad (1)$$

This reaction implies that both the magma and country rock deliver 50% of the oxygen for the andradite formation. Consequently skarn-related grandites (and the skarn itself) should have $\delta^{18}O_{SMOW}$ values between 10 and 20‰. These values were calculated under the assumption that the carbonate has $\delta^{18}O_{SMOW}$ values between 13 and 33‰ (Fulignati et al. 2005; Gilg et al. 2001), the $\delta^{18}O_{SMOW}$ values for the magmatic fluid are between 7 and 8‰ and the marble/fluid (R/W) ratio is ~1. On the basis of the $\delta^{18}O_{SMOW}$ values from Mt. Somma-Vesuvius skarns (11.8–16.4‰) we have to proceed on the assumption that the rock/water ratios

Table 4 $\delta^{18}O_{V\text{-}SMOW}$ and $^{87}Sr/^{86}Sr$ isotope composition for (a) Mercato and Avellino whole-rocks, (b) Mercato base and Avellino 7 minerals

(a) Whole-rocks

Sample	Geochemical classification	$\delta^{18}O_{V\text{-}SMOW}$	$^{87}Sr/^{86}Sr$	Reference
Mercato base	Phonolitic pumice	9.5 ± 0.2‰	0.70725 ± 1	Oxygen isotopes (Ayuso et al. 1998)
Avellino 3	Phonolitic pumice	9.8 ± 0.2‰	0.70729 ± 1	Oxygen isotopes (Ayuso et al. 1998)
Avellino 7	Tephri-phonolitic pumice	8.8 ± 0.2‰	0.70769 ± 1	Oxygen isotopes (Ayuso et al. 1998)

(b) Minerals

Sample	No. of mineral	$\delta^{18}O_{V\text{-}SMOW}$	$^{87}Sr/^{86}Sr$
Mercato base	Mineral separate		
Titanian andradite	# 1	8.0 ± 0.2‰	0.70724 ± 1
Titanian andradite	# 2	7.2 ± 0. 2‰	
Titanian andradite	# 3	7.9 ± 0. 2‰	
Titanian andradite	# 4	8.5 ± 0.2‰	
Titanian andradite	# 5	7.4 ± 0.2‰	
Titanian andradite	# 6	7.2 ± 0.2‰	
Titanian andradite	# 7	6.8 ± 0.2‰	
Avellino 3			
Titanian andradite	# 1	7.9 ± 0.2‰	0.70729 ± 1
Titanian andradite	# 2	7.4 ± 0.2‰	
Titanian andradite	# 3	7.1 ± 0.2‰	
Titanian andradite	# 4	7.9 ± 0.2‰	
Sanidine	# 1	9.9 ± 0.2‰	

Data are from that study if not referenced from elsewhere

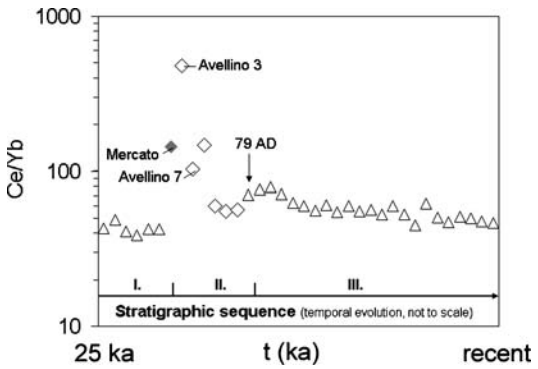

Fig. 7 Magmas from parts of Avellino and Mercato pumice sequences show higher Ce/Yb-ratios than all other eruptions of Mt. Somma-Vesuvius, which can only be explained by significant removal of grandites or other accessory mineral phases out of the melt (see text for discussion). Data are from this study, Ayuso et al. (1998) and Somma et al. (2001). *White diamond* Avellino, *grey diamonds* Mercato, *diamonds* Pre-Mercato and Post-Avellino, *I*, *II*, *III* geochemical groups of Mt. Somma-Vesuvius—see Fig. 2

ranged between 0.3 and 1.5 during the carbonate–magmatic fluid interaction. Skarn-derived grandites should have $\delta^{18}O_{SMOW}$ values between 9 and 14‰, which is in contrast to the measured $\delta^{18}O_{SMOW}$ values between 7 and 8‰ (Table 4) for the grandites of this study.

Note that the $\delta^{18}O_{SMOW}$ value for the magmatic fluid is a minimal value. In previous studies it was shown that the $\delta^{18}O_{SMOW}$ values of the magmatic fluid increase (1) during the exsolution of the fluid from alkaline magmas in a shallow magma chamber and/or (2) during interaction between the magmatic fluid and country rock producing a Na–K–Ca carbonate–chloride rich melt (Fulignati et al. 2005). H_2O-rich magmatic fluids from Mercato and Avellino 3 magma, which have reacted with the carbonate country rock, show for example (calculated) $\delta^{18}O_{SMOW}$ values between +10‰ (Fulignati et al. 2005) and +12 ± 1‰ (Gilg et al. 2001). These values are reasonable if the magmatic fluid was produced at a temperature between 700 and 850°C, the host magma had a $\delta^{18}O_{SMOW}$ value of ~8‰ and the wall rock marble had a $\delta^{18}O_{SMOW}$ value of ~28‰. Thus, skarn-related grandite forming processes with contaminated magmatic fluid would further increase the $\delta^{18}O_{SMOW}$ values of the skarn-related grandites.

The grandites of Mercato and Avellino 3 have lower $\delta^{18}O_{SMOW}$ values (6.8 to 7.9 ± 0.4) than the magmatic fluids, marble and skarn. Furthermore, the grandites show identical or lower $\delta^{18}O_{SMOW}$ values than their host melt (7–9‰; Turi and Taylor 1976; Ayuso et al. 1998) (Fig. 8). On the basis of the oxygen isotope composition of the host melt it appears that Mercato

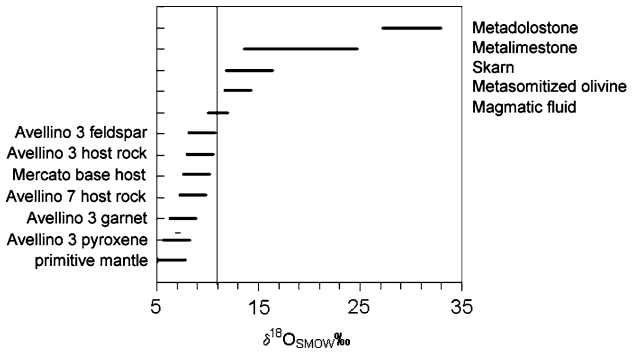

Fig. 8 $\delta^{18}O_{SMOW}$ values for Avellino 3 minerals, host rock, magmatic fluid (references see text) and wallrock (Gilg et al. 2001)

and Avellino 3 are of magmatic origin. The lower $\delta^{18}O_{SMOW}$ values of the grandites with respect to their host melt can be explained by increasing crustal assimilation after (or during) the grandite crystallization (Ayuso et al. 1998). This is also indicated by the elevated $\delta^{18}O_{SMOW}$ values of other late-stage minerals of Avellino 3 like the feldspar (9.9‰).

Previous studies pointed out that the strontium isotope composition of the Mt. Somma-Vesuvius system is less indicative for discrimination between magmatic and skarn-related processes, because of the variable and similar isotope composition of the wall rock and the phonolitic melt (e.g. Fulignati et al. 2005). However, when directly compared, Mercato and Avellino 3 grandites show similar strontium isotope composition compared to their host melt (0.70725 and 0.70729), but different Sr isotope ratios than the marble (0.70756; Gilg et al. 2001). Furthermore, the quantity of strontium in Mercato and Avellino 3 whole-rocks (Mercato: 17 ppm, Avellino 3: 171 ppm) are much lower than in the wall-rock (300–1,000 ppm, Civetta et al. 1991). Hence, skarn-related garnets should reflect the Sr isotope ratios of the marble rather than that of the magmatic fluid, even implying a large variation in the Sr isotope ratios of the garnets in dependence of the rock/fluid ratio. We do not observe such a variation; thus Sr isotopes also indicate that Mercato and Avellino garnets are of igneous origin.

Partition coefficients and major and rare earth element zoning

Having established that Mercato grandites are of magmatic origin, the question arises whether they were formed in the host melt or derived from an older magma. We have several indications that they are juvenile to the erupted pumices: all Mercato crystals are euhedral with no evidence of resorption boundaries or resorbed cores (Fig. 4). They are completely unzoned and homogeneous in major- and trace elements. An incorporation of older grandites into a juvenile magma should lead to resorption or regrowth of the xenocrysts. It is not likely that the new magma batch, which incorporated the grandites, had exactly the same temperature, oxygen fugacity, fractionation degree, and isotope composition as the resident magma. Additionally, the melt (glass) of Mercato is characterized by a depletion of the heavy rare earth elements with respect to other Vesuvius phonolites and their parent melts implying an impoverishment of the Mercato melt by an HREE-rich phase, such as garnet. Such HREE-depletion is not observed in other Vesuvius phonolites except for the second garnet-bearing phonolite from the Avellino 3 eruption. HREE are known to substitute for major divalent cations in the large dodecahedral garnet X site (Westrenen et al. 2001). Taken together, these observations are all consistent with an in-situ equilibrium growth of garnets from the phono-tephritic host melt.

Additionally the REE-signature from the grossularite-rich garnets of Mercato is distinctly different from e.g. pyrope-rich garnets, because of their flat patterns between Sm and Lu (Fig. 10a). These patterns are in consistent with experimental studies (Westrenen et al. 1999, 2001), which demonstrated that grossularite-rich garnets have only limited potential to fractionate the HREE compared to e.g. pyrope-rich garnets.

Both Mercato and Avellino garnets have the same CaO content (31.2–32.2%) but major differences in their HREE budget. Hence, the effect of major element composition of garnets (e.g. CaO content) cannot be the cause for the variations in HREE of Mercato and Avellino 3 garnets. Alternative explanations e.g. open system magma differentiation processes need to be considered for Avellino 3 melts.

Calculated partition coefficients for Mercato andradites and host melt (glass) with $D^{Grt/Melt}$ (La) = 0.5, $D^{Grt/Melt}$ (Sm) = 48 and $D^{Grt/Melt}$ (Yb) = 110 (Table 5) accord with previous in-situ and experimental studies on partitioning between igneous garnet and their differentiated host melt (dacite: Irving and Frey 1978; rhyolite: Sisson and Bacon 1992). Note, however that the grandites from phonolites have a higher preference for Sm and middle REE compared to garnets grown from a dacitic or rhyolitic melt (Fig. 9).

In contrast, all grandites in Avellino 3 pumices are zoned. Most of the grandite grains show zoning at two length scales: a large-scale zonation with a wavelength of ~100 μm and a oscillation at a few micrometres up to tens of micrometres. The compositional changes at

Table 5 Partition coefficient for rare earth elements between grandites and a phonolitic melt (Mercato base pumice)

	Mean partition coefficient $D_{Grt/phonolitic\ melt}$	Range of partition coefficients between the several garnets
La	0.5	0.5–0.7
Ce	2	1.9–2.4
Pr	6	5.1–6.0
Nd	15	13.7–15.6
Sm	48	44–52
Gd	44	40–49
Tb	78	71–88
Dy	102	94–119
Er	107	95–130
Tm	107	96–129
Yb	110	97–124

Analytical uncertainty: ±20%

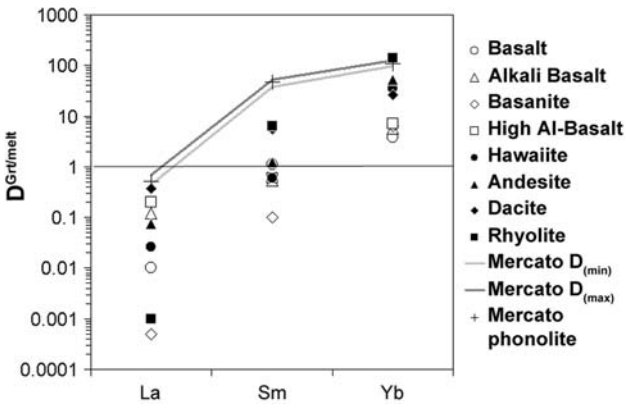

Fig. 9 The diagram shows literature data for partition coefficients between garnet and melts of different compositions. Data are from Geochemical Earth Reference Model (GERM) database (http://www.earthref.org)—Basalt: Hauri et al. (1994); Alkali Basalt: Shimizu (1974); Basanite: Irving and Frey (1978); High Al-Basalt: Shimuzu (1974); Hawaiite, Andesite, Dacite: Irving and Frey (1978); Rhyolite: Sisson and Bacon (1992)

both scales are discrete and mostly with sharp boundaries (Fig. 5). None of the grains show evidence for diffusion processes between the individual zones due to the lack of diffuse smoothing of compositional boundaries between the zones. The major part of the grains shows dark Al-rich cores ($Gro_{38}And_{62}$ to $Gro_{40}And_{60}$), sometimes with traces of resorption. The overgrowths on the cores are variable in their Al–Fe-composition. Some overgrowths have more Al than the cores ($Gro_{45}And_{55}$), some show the same composition in Al and Fe, and some are Fe-rich ($Gro_{33}And_{67}$). It appears that these grandites crystallized under different conditions in the magma. For example, grandites prefer to incorporate Fe over Al at higher temperature (Meagher 1982) and pressure. In addition, an increase of the oxygen fugacity in the melt favours the presence of threefold charged iron ions in the melt, which should favour the incorporation of Fe^{3+} more than Al^{2+} into the octahedral position of the garnet.

Zonation and resorption of Avellino 3 grandites could indicate a xenocrystic origin. However, on the basis of (1) the depletion in HREE of several Avellino 3 minerals, such as the garnet, magmatic amphibole and magmatic pyroxene, (2) the similar strontium isotope composition of their host rock and (3) the increasing depletion history of Avellino 3 melt in HREE, we favour a magmatic origin for Avellino 3 grandites as well. Variable depletion in HREE of the Avellino grandites grains (AV-2 to AV-5) can be classified into four stages (Fig. 10). Based on this observation a model is developed for the crystallization environment of Avellino 3 grandites, which describes a continuous HREE-depletion of the Avellino 3 melt during a discontinuous growth of the single garnet grains:

Stage 1 grandite grains show a Fe-rich core with REE element pattern similar to grandites in Mercato pumice with typical low Sm/Yb = 3 for Ca-rich garnets. The crystals have Al-rich overgrowths with higher Sm/Yb ratios (5–6) than in the Fe-rich core (Figs. 6a, 10a). The *second stage* grandite shows Al-rich cores with low Sm/Yb-ratios (5–8) and Fe-rich rims with Sm/Yb-ratios between 37 and 155 (Figs. 6b, 10b). The Al-rich core was affected by resorption processes. *Stage 3* grandite is Al-rich in its core and rim. Sm/Yb-ratios are lower in the core (Sm/Yb = 15–55) than in the rim (Sm/Yb = 82–106) (Figs. 6c, 10c). *Stage 4* grandite shows an Al-rich core with Sm/Yb-ratios between 62 and 180 and Sm/Yb-ratios up to 420–844 in the Fe-rich rim (Figs. 6d, 10d). The cores of grandite types 1, 3 and 4 show no evidence of resorption for the major parts of the cores. Overall, there is a decrease in HREE from core to rim, from one garnet to the next and a progressive decrease in HREE in Avellino 3 melt. Such HREE depleted patterns (Fig. 10), such as in the late-stage grandites (Stages 2–4), are very unusual for grandites. One possible explanation is the crystallization of late-stage grandites (Stages 2–4) from a melt that was previously extremely depleted in HREE by prior grandite fractionation (e.g. Stage 1). Furthermore, it appears that the processes, which are controlling the Al/Fe ratio in the grandite zones are connected with the ongoing HREE depletion of Avellino 3 melt. The core of the less evolved grandite (*Stage 1*) is Fe-rich, the rims and cores with similar moderate HREE-depletion (Sm/Yb = 5–8) are Al-rich. The rim of the highest evolved late-stage grandite (*Stage 4*) is again Fe-rich.

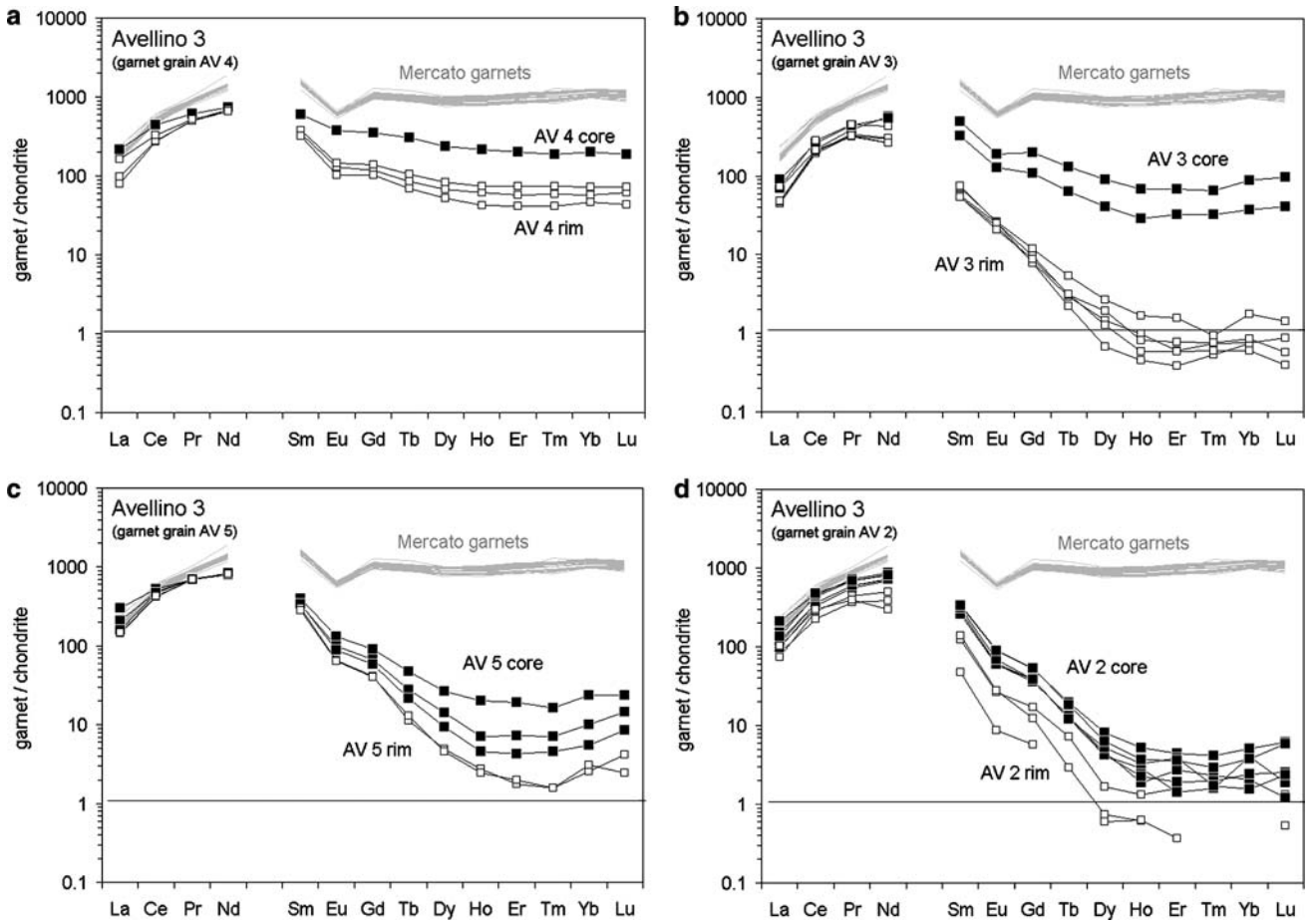

Fig. 10 REE element patterns for the different stages of development from 1 to 4 (a–d) of Avellino grandites. Explanations see text. *Black squares* REE data from Avellino garnet cores, *white squares* REE data from Avellino garnet rims, *grey* REE from Mercato garnet

The stepwise HREE depletion of the grandites from core to rim can be ascribed to the following process. The core of a grandite similar to those found in Mercato with a ''normal'' HEE garnet signature, such as the Mercato garnets, was removed from the HREE-depleted residual melt by crystal settling. This was followed by the growth of an HREE-depleted rim from an even more HREE-depleted residual melt (Fig. 10a). Such HREE depleted melt may have formed from previous fractionation of garnet or other accessory mineral phases. In an alternative view, the core of the grandite was not removed from the melt but instead the growth of the garnet was not continuous and the Avellino melt was depleted in HREE by other accessory mineral phases during the stagnation of the growth of single grandite grains.

Such an accessory phase has to show an affinity to the REE and a strong preference for HREE over LREE. Accessory mineral phases, which crystallize during late-stage magma evolution and prefer HREE are zircon or xenotime. It is in fact possible that zircon precipitated out of highly evolved Avellino melts (>57% SiO_2), because of the observed Zr depletion in the Avellino melt. However, experiments with granitic melts characterized by the same molar Al/(Na+K) ratio than the melts of Avellino 3 (molar Al/(Na + K) ratio of Avellino 3 = 0.93) indicate a solubility of up to 3,500 ppm ZrO_2 at 800°C and 200 MPa (Linnen and Keppler 2002; Watson and Harrison 1983). The highest zirconium concentrations found in Avellino eruption products is less than 960 ppm, which is too low to allow zircon saturation in Avellino melts.

Other mineral phases that have the potential to lower Zr concentrations in a melt significantly are titanite or the grandites themselves. Experimental studies with a basaltic melt and Ca-rich garnets (Ca > 20 wt%) indicated that zirconium is compatible in calcic garnets with $D_{Zr}^{Grt/melt}$ between 2 and 4 (Westrenen et al. 2001 and references herein). Thus, the calculated partition coefficients for zirconium between

Avellino garnets and Avellino 3 glass of this study ($D_{Zr}^{Grt/melt}$ = 2.0 to 3.5) suggest that the grandites in fact do have the potential to lower the zirconium content in residual Avellino 3 melt.

In order to test if grandite (and zircon) crystallization can raise the Sm/Yb ratios in the Avellino grandites to the extent observed, and whether the HREE-depletion was caused by magmatic processes, we modelled the variation of Sm/Yb for melts and garnets during crystal fractionation. Note that the large variation in HREE of Avellino grandites indicates crystallisation in disequilibrium, unlike that for the Mercato grandites. The extensive and progressive depletion in HREE of the Avellino 3 grandites from core to rim requires Rayleigh fractionation for their formation and hence we used the formula for Rayleigh fractionation for modelling crystal fractionation.

We present five calculations with different types and proportions of crystallizing minerals (Fig. 11). In detail, we calculated the initial Sm and Yb concentrations (C_i) of Avellino melts, which were in equilibrium with the individual Avellino grandite zones. For doing so, we used the partition coefficient from the *Mercato grandite–Mercato phonolitic melt* pair of this study. It follows that a hypothetical Avellino melt 1, from which grandites crystallized with high amounts of HREE (core, *Stage 1*), show concentrations $c_{i,High}$ for Sm of 1.9 ppm and for Yb of 0.3 ppm. In contrast, strongly HREE-depleted rims must derive from a strongly HREE-depleted Avellino melt ''X'' that should have $c_{i,Low}$ for Sm of 1 ppm and for Yb of 0.03 ppm. Note, that Avellino 3 glass and Avellino 3 whole-rock show Sm and Yb concentrations between $c_{i,High}$ and $c_{i,Low}$ (Table 2), indicating that Avellino 3 melt was variably depleted in HREE by grandites (and other mineral phases, such as zircon or xenotime). Avellino 3 melt may then be a mixture of different melt fractions that were variably depleted in HREE.

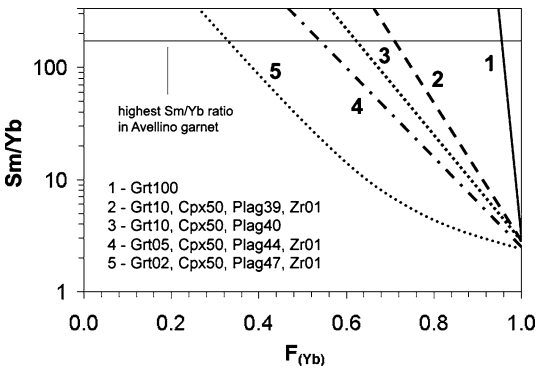

Fig. 11 Calculation of the variation of the Sm/Yb ratios during Rayleigh crystal fractionation in Avellino 3 melt. The calculation was done for five different compositions of the cumulate. The numbers after the mineral type gives the proportion of the cumulate, e.g. Grt10, Cpx50, Plag39, Zr01 = 10% garnet, 50% clinopyroxene, 39% plagioclase and 1% zircon. Further explanations see text

Our model quantifies the fraction and composition of crystallizing minerals, which raise the Sm/Yb ratio of melt ''1'' (Sm/Yb = 3) to Sm/Yb ratios in a melt ''X'' (Sm/Yb up to ~180). If other minerals with low $D_{REE}^{crystal/melt}$ crystallized together with the grandites, then the effect of depleting the melt in HREE is dampened. For the determination of bulk partition coefficients we used our partition coefficients for grandites, for amphibole those of Adam and Green (1994), for clinopyroxene from Mahood and Stimac (1990) and for plagioclase and zircon from Nagasawa (1970). If the fractionating assemblage consists of 100% garnet, then only 3–4% crystallisation would be required to explain the variation in Sm/Yb as calculated from the garnet compositions. If, however, feldspars and pyroxenes dominate the crystallization assemblage, than the required amount would be much higher: 30–67% cumulate for 2–10% of garnet and less than 1% of zirconium in it (Fig. 11).

The question remains, why the phonolitic magmas of Avellino and Mercato were affected by different fractionation regimes resulting in disequilibrium zoned garnets and equilibrium unzoned garnets. One explanation is that the phonolitic magma of Avellino 3 was repeatedly underplated by trachytic magma of Avellino 7. The arrival of a hotter magma to a colder residing magma may have triggered or enhanced the convection in the colder Avellino 3 magma chamber leading to discontinuous growth. This model agrees with the history of magma refilling of the Vesuvius magma chamber (e.g. Civetta et al. 1991; Cioni et al. 1995) resulting from crystallization and mixing processes related to the periodic supply of mafic magma batches. In contrast, all Mercato eruption products show a narrow range for their degree of fractionation. Hence, it appears that the Mercato magma chamber was not affected by replenishment with hotter and more mafic magma.

Clinopyroxene and co-genetic HREE-depleted amphibole

For verifying the magmatic origin of the Avellino grandites and for tracing the times and processes of HREE depletion during the magma evolution, it is useful to study the REE patterns in other minerals, such as clinopyroxene and amphibole (mineral compositions, see Fig. 12). Cioni et al. (1999a) showed for the Mt. Somma-Vesuvius magma system, that the en-

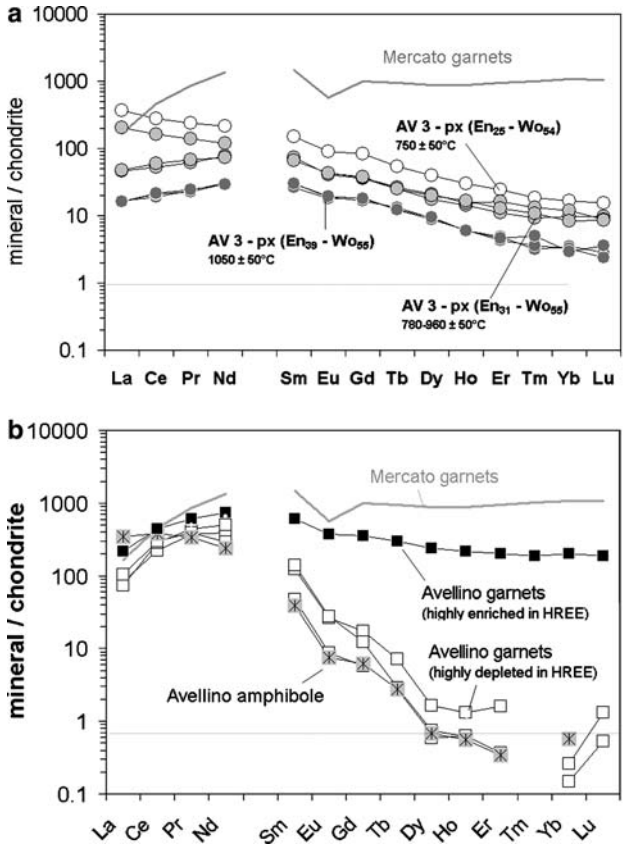

Fig. 12 REE patterns for **a** pyroxene and **b** amphibole show that amphibole was derived from a HREE-depleted melt, whereas the pyroxene formed prior to HREE fractionation by garnet growth. Legend see figure

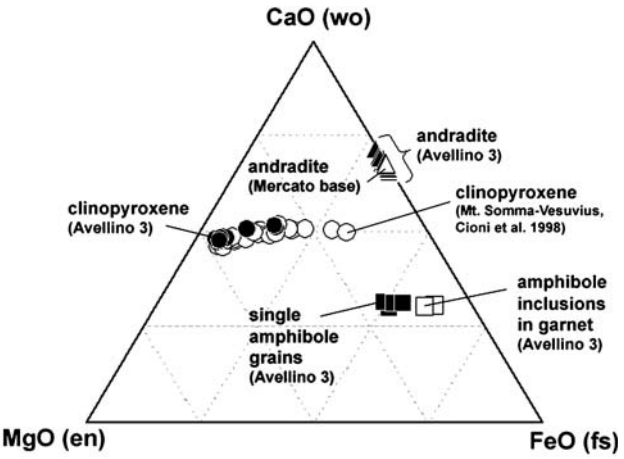

Fig. 13 Major element compositions of clinopyroxene and amphiboles and the grandites from Mercato and Avellino expressed as atomic percent of Mg, Fe and Ca illustrating the composition of Avellino 3. For reference the composition and evolution path of clinopyroxenes of Mt. Somma-Vesuvius are given (Cioni et al. 1999a). Ideal end-member compositions for pyroxene are given with enstatite (en)—wollastonite (wo) and ferrosilite (fs). Legend see figure

statite component of pyroxenes is a function of crystallisation temperature. Hence, the enstatite fraction of Avellino 3 pyroxenes and inclusions in garnets can be used directly as a geothermometer for their host melt. On the basis of this geothermometer it appears that Avellino clinopyroxenes (En_{39}–Wo_{55} to En_{25}–Wo_{54}) were formed during a wide temperature range between 1,050 and 750 ± 50°C. The REE concentrations in the clinopyroxenes increase from the high-temperature to the low-temperature clinopyroxenes more than 10 times (Fig. 13a). This is caused by REE enrichment in the melt during cooling and crystal fractionation. The clinopyroxenes show no significant depletion in HREE relative to typical REE patterns for clinopyroxene. Hence it appears that they are early phases and derived from a melt, which was not yet significantly depleted in HREE.

In contrast, the amphiboles of Avellino 3 and the amphibole inclusion of Avellino 3 grandites are strongly depleted in HREE relative to typical amphibole REE patterns (Fig. 13b). These HREE patterns were apparently produced during amphibole crystallization out of a strongly HREE-depleted melt, indicating that amphibole crystallization occurred at a late-stage during or after grandite crystallization.

Conclusions

1. Grandites from the pre-historic Mt. Somma-Vesuvius phonolite-magma system are of magmatic origin. For classifying the grandites it is required to apply multiple criteria, such as colour, major- and trace element, and isotope composition. The high TiO_2, the high-temperature mineral inclusions and the magmatic Sr and O isotope compositions, all support the magmatic origin of the Mt. Somma-Vesuvius grandites.
2. Grandites from phonolitic Mercato melt are unzoned and homogeneous in their major- and trace elements and formed in equilibrium in a large closed homogeneous magma chamber. Their uniform REE patterns indicate crystallisation in a closed system and no additional accessory HREE-rich mineral phase crystallized during the grandite formation. This homogeneity of the grandites allows calculation of reliable empirical partition coefficient between grandites and the Mercato phonolitic melt. Additionally the grossularite-rich garnets of Mercato show flat patterns between Sm and Lu (Fig. 10a), which is in consistent with previous experimental studies. This implies that

grossularite-rich garnets has not the potential to fractionate the HREE such as e.g. pyrope-rich garnets.

3. In contrast, Avellino 3 grandites are zoned and heterogeneous in their major- and trace elements. The rims of Avellino 3 grandites and other cogenetic minerals (amphibole) show significant HREE depletions, which can only be explained by crystallisation from an HREE-depleted melt. The grandites were formed in a magma chamber, which was affected by extensive HREE removal via grandites and/or other accessory mineral phases. Convection triggered by the replenishment with hotter tephritic Avellino 7 magma may have been responsible for rapid disequilibrium growth and transfer of phenocrysts into different magma batches with different HREE content.
4. The evolution of Avellino 3 magma started first with the crystallization of high-temperature minerals, such as pyroxene (>1,050°C) in a large open magma chamber. Subsequently, the Avellino melt in the magma chamber cooled down to a temperature at which grandites, amphibole, low-temperature pyroxenes and other mineral phases started to grow (<750°C). A step-wise decrease in Sm/Yb ratios of the garnets and the different stages of HREE-depletion in Avellino garnets however, indicates that the Avellino grandites did not grow continuously but derived from a melt, which was progressively impoverished in HREE step less.

Acknowledgment We are grateful to the members of the Osservatorio Vesuviano for selecting samples and showing appropriated outcrops for sampling Mercato and Avellino pumices. For technical assistance we thank Reinhold Przybilla, Gaby Mengel, Angelika Reitz, Erwin Schiffcyk and Ingrid Reuber. B.S. is particularly grateful to Dan Morgan and Burkhard Schmidt for fruitful discussions about the origin and growth of grandites in a skarn-forming environment. We are also indebted to T.L. Grove, Trevor Green and Roberto Ayuso for very constructive comments. This study was funded by the 5th Framework Programme of the European Union within the ERUPT project. We thank in particular Jon Davidson for setting up and leading the ERUPT project.

References

Adam J, Green TH (1994) The effects of pressure and temperature on the partitioning of Ti, Sr and REE between amphibole, clinopyroxene and basanitic melts. Chem Geol 117:219–233

Amthauer G, Annersten H, Hafner SS (1977) The Mössbauer spectrum of ^{57}Fe in titanium-bearing andradites. Phys Chem Miner 1:399–413

Armbruster T, Birrer J, Libowitzky E, Beran A (1998) Crystal chemistry of T-bearing andradites. Eur J Mineral 5:907–921

Aulinas M, Civetta L, Di Vito M, Orsi G, Gimeno D, Fernandez JL, Fernanadez Turiel JL (2007) The Plinian Mercato eruption of Mt. Somma-Vesuvius: magma chamber processes and eruption dynamics. Bull Volcanol (in press)

Ayuso AA, De Vivo B, Rolandi G, Seal II R, Paone A (1998) Geochemical and isotope (Nd-Pb-Sr-O) variations bearing on the genesis of volcanic rocks from Vesuvius, Italy. J Volcanol Geotherm Res 82:53–78

Cioni R (2000) Volatile content and degassing processes in the AD 79 magma chamber at Vesuvius (Italy). Contrib Mineral Petrol 140:40–54

Cioni R, Civetta L, Marianelli P, Metrich N, Santacroce R, Sbrana A (1995) Compositional layering and syn-eruptive mixing on a periodically refilled shallow magma chamber: the AD 79 Plinian eruption of Vesuvius. J Petrol 36:739–776

Cioni R, Marianelli P, Santacroce R (1998) Thermal and compositional evolution of the shallow magma chambers of Vesuvius: evidence from pyroxene phenocrysts and melt inclusions. J Geophys Res Solid Earth 103:18277–18297

Cioni R, Marianelli P, Santacroce R (1999a) Temperature of Vesuvius magmas. Geology 27:443–446

Cioni R, Santacroce R, Sbrana A (1999b) Pyroclastic deposits as a guide for reconstructing the multi-stage evolution of the Mt. Somma-Vesuvius Caldera. Bull Volcanol 60:207–222

Civetta L, Orsi G, Scandone P, Pece R (1978) Eastwards migration of the Tuscan anatectic magmatism due to anticlockwise rotation on the Apennines. Nature 279:604–605

Civetta L, Galati R, Santacroce R (1991) Magma mixing and convective compositional layering within the Vesuvius magma chamber. Bull Volcanol 53:287–300

Civetta L, D'Antonio M, De Lorenzo S, Di Rienzo V, Gasparini P (2004) Thermal and geochemical constrains on the ''deep'' magmatic structure of Mt. Vesuvius. J Vocanol Geotherm Res 133:1–12

D'Antonio M, Tonarini S, Arienzo I, Civetta L, Di Renzo V (2007) Components and processes in the magma genesis of the Phlegrean Volcanic District. Bull Geol Soc Am (in press)

De Natale G, Troise C, Pingue F, Mastrolorenzo G, Pappalardo L (2006) The Somma-Vesuvius volcano (Southern Italy): structure, dynamics and hazard evaluation. Earth Sci Rev 74:73–111

De Vivo B, Rolandi G, Gans PB, Calvert A, Bohrson WA, Spera FJ, Belkin HE (2001) New constraints on the pyroclastic eruptive history of the Campanian volcanic Plain (Italy). Mineral Petrol 73:47–65

Dorendorf F, Wiechert U, Wörner G (2000) Hydrated sub-arc mantle: a source for the Kluchevskoy volcano, Kamchatka/Russia. Earth Planet Sci Lett 175:69–86

Elter P, Grasso M, Parotto M, Mezzani L (2003) Structural setting of the Apennine-Maghrebian thrust belt. Episodes 26:205–211

Ferguson LJ and Edgar AD (1978) Petrogenesis and origin of analcime in volcanic-rocks of Crows-Nest formation, Alberta. Can J Earth Sci 15:66–77

Fulignati P, Marianelli P, Santacroce R, Sbrana A (2004) Probing the Vesuvius magma chamber–host rock interface through xenoliths. Geol Mag 141:417–428

Fulignati P, Panichi C, Sbrana A, Caliro S, Gioncada A, Del Moro A (2005) Skarn formation at the walls of the 79 AD magma chamber of Vesuvius (Italy): mineralogical and isotope constraints. Neues Jahrbuch der Mineralogie (Abhandlungen) 181:53–66

Gilg HA, Lima A, Somma R, Belkin HE, De Vivo B, Ayuso RA (2001) Isotope geochemistry and fluid inclusion study of skarns from Vesuvius. Mineral Petrol 73:145–176

Gomes CDB (1969) Electron microprobe analysis of zoned melanites. Am Mineral 54:1654–1669
Green TH (1977) Garnet in silicic liquids and its possible use as a P–T indicator. Contrib Mineral Petrol 65:59–67
Guest J, Cole P, Duncan A, Chester D (2003) Volcanoes of Southern Italy. The Geological Society Publishing House, London, pp 284
Hartmann G (1994) Late-medieval glass manufacture in the Eichsfeld Region (Thuringia, Germany). Chemie der Erde 54:103–128
Hauri EH, Wagner TP, Grove TL (1994) Experimental and natural partitioning of Th, U, Pb and other trace elements between garnet, clinopyroxene and basaltic melts. Chem Geol 117:149–166
Huggins FE, Virgo D, Huckenholz HG (1977) Titanium containing silicate garnets II. The crystal chemistry of melanites and schorlomites. Am Mineral 62:646–665
Irving AJ and Frey FA (1978) Distribution of trace-elements between garnet megacrysts and host volcanic liquids of Kimberlite to Rhyolitic composition. Geochimica et Cosmochimica Acta 42:771–787
Johnson KTM, (1998) Experimental determination of partition coefficients for rare earth and high-field-strength elements between clinopyroxene, garnet, and basaltic melt at high pressure. Contrib Mineral Petrol 133:60–68
Kohn MJ and Valley JW (1998) Effects of cation substitution in garnet and pyroxene on equilibrium oxygen isotope fractionations. J Metamorph Geol 16:625–639
Lackey JS, Valley JW, Hinke HJ (2006) Deciphering the source and contamination history of peraluminous magmas using $\delta^{18}O$ of accessory minerals: examples from garnet-bearng plutons of the Sierra Nevada batholith. Contrib Mineral Petrol 151:20–44
Lang JR, Lueck B, Mortensen JK (1995) Triassic-Jurassic silica-undersaturated and silica-saturated alkalic intrusions in the Cordillera of British-Columbia—implications for arc magmatism. Geology 23:451–454
Lavecchia G and Stoppa F (1996) The tectonic significance of Italian magmatism: an alternative view to the popular interpretation. Terra Nova 8:435–446
Lima A, Danyueshevsky LV, De Vivo B, Fedele L (2003) A model for the evolution of the Mt. Somma-Vesuvius magmatic system based on fluid and melt inclusions investigations. In: De Vivo B, Bodran RJ (eds) Melts inclusions in volcanic systems: methods, applications and problems. Series development in Volcanology. Elsevier, Amsterdam, pp 227–249
Linnen RL, Keppler H (2002) Melt composition control of Zr/Hf fractionation in magamtic processes. Geochimica et Cosmochimica Acta 66:3293–3301
Mahood GA, Stimac JA (1990) Trace-element partitioning in pantellerites and trachytes. Geochimica et Cosmochimica Acta 54:2257–2276
Meagher EP (1982) Silicate garnets. In: Ribbe PH (ed) Orthosilicates, 2nd edn. Rev Mineral Geochem 5:25–66
Nagasawa H (1970) Rare Earth concentrations in zircon and apatite and their host dacite and granites. Earth Planet Sci Lett 9:359–364
Naimo D, Balassone G, Beran A, Amalfitano C, Imperato M, Stanzione D (2003) Garnets in volcanic breccias of the Phlegraean Fields (southern Italy): mineralogical, geochemical and genetic features. Mineral Petrol 77:256–270
Orsi G, de Vita S, Di Vito M (1996) The restless, resurgent Campi Flegrei nested caldera (Italy): constraints on its evolution and configuration. J Volcanol Geotherm Res 74:179–214
Paone A (2004) Evidence of crustal contamination, sediment, and fluid components in the Campanian volcanic rocks. J Volcanol Geotherm Res 138:1–26
Peccerillo A (1999) Multiple mantle metasomatism in central-southern Italy: geochemical effects, timing and geodynamic implications. Geology 27:315–318
Pertermann M, Hirschmann MM, Hametner K, Günther D, Schmidt MW (2004) Experimental determination of trace element partitioning between garnet and silica-rich liquid during anhydrous partial melting of MORB-like eclogite. Geochem Geophys Geosyst 5:2003GC000638
Rocholl A, Dulski P, Raczek I (1997) Chemical characterisation of NIST silicate glass certificate reference material SRM 610 by ICP-MS, TIMS, LIMS, SSMS, INAA, AAS and PIXE. Geostand Newsl 21:101
Russell JK, Dipple GM, Lang JR, Lueck B (1999) Major-element discrimination of titanian andradites from magmatic and hydrothermal environments: an example from the Canadian Cordillera. Eur J Mineral 6:919–935
Salters VJM and Longhi J (1999) Trace element partitioning during the inital stages of melting beneath mid-ocean ridges. Earth Planet Sci Lett 166:15–30
Santacroce R (1983) A general model for the behaviour of the Somma Vesuvius volcanic complex. J Volcanol Geotherm Res 17:237–248
Scaillet B and Pichavant M (2004) Crystallisation conditions of Vesuvius phonolites. Geophys Res Abstr 6:03764
Scordari F, Schingaro E, Pedrazzi G (1999) Crustal chemistry of melanites from Mt. Vulture (Southern Italy). Eur J Mineral 11:855–869
Shimizu N (1974) An experimental study of the partitioning of K, Rb, Cs, Sr, and Ba between clinopyroxene and liquid at high pressures. Geochimica et Cosmochimica Acta 38:1789–1798
Sisson TW, Bacon CR (1992) Garnet—high-silica rhyolite trace-element partition coefficients measured by ion microprobe. Geochimica et Cosmochimica Acta 56:2133–2136
Smith MP, Henderson P, Jeffries TER, Long J, Williams CT (2004) The rare earth elements and uranium in garnets from the Beinn and Dubhaich Aureole Skye, Scotland, UK: constraints on Processes in a dynamic hydrothermal system. J Petrol 45:457–484
Somma R, Ayuso RA, De Vivo B, Rolandi G (2001) Major, trace element and isotope geochemistry (Sr-Nd-Pb) of interplinian magmas from Mt. Somma-Vesuvius (Southern Italy). Mineral Petrol 73:121–143
Turbeville BN (1993) Sidewall differentiation in an alkalic magma chamber—evidence from syenite in tuffs of the Latera Caldera, Italy. Geol Mag 130:453–470
Turi B, Taylor HP (1976) Oxygen isotope studies of potassic volcanic rocks of Roman Province, Central Italy. Contrib Mineral Petrol 55:1–36
Valley JW, Kitchen N, Kohn MJ, Niendorf CR, Spicuzza MJ (1995) UWG-2, a garnet standard for oxygen isotope ratios: strategies for high precision and accuracy with laser heating. Geochimica et Cosmochimica Acta 59:5223–5231
Vielzeuf D, Vechambre M, Brunet F (2005) Oxygen isotope heterogenieties and diffusional profiles in composite metamorphic/magamtic garnets from the Pyrenees. Am Mineral 90:463–472
Watson EB, Harrison TM (1983) Zircon saturation revisited: temperature and composition effects in a variety of crustal magma types. Earth Planet Sci Lett 64:295–304
Westrenen W, Blundy J, Wood B (1999) Crystal-chemical controls on trace element partitioning between garnet and anhydrous silicate melt. Am Mineral 84:838–847

Westrenen W, Blundy JD, Wood BJ (2001) High field strength element/rare earth element fractionation during partial melting in the presence of garnet: implications for identification of mantle heterogeneities. Geochem Geophys Geosyst 2. doi:2000GC000133

Zollo A et al (1996) Seismic evidence for a low-velocity zone in the upper crust beneath Mount Vesuvius. Science 274:592–594